

# 1 **Anomalous structure of MgCO<sub>3</sub> liquid and the buoyancy of carbonatite melts**

2 Sean M. Hurt<sup>a, b\*</sup> and Aaron S. Wolf<sup>a</sup>

3 *\*Corresponding author email address: seanhurt@umich.edu*

4 <sup>a</sup> Department of Earth and Environmental Sciences, University of Michigan, 1100 N. University Ave., Room 2534,  
5 Ann Arbor, MI 48109, USA

6 <sup>b</sup> Division of Math and Science, Nation Park College, 101 College Dr., Hot Springs National Park, AR 71913, USA

7  
8 *[This preprint has been submitted to Earth and Planetary Science Letters]*

## 9 10 **Key Points**

- 11 • The structure of MgCO<sub>3</sub> liquid is unique among the other alkaline earth carbonates.
- 12 • Mg<sup>2+</sup> adopts anomalously low 4-fold coordination with O<sub>2</sub><sup>-</sup> and CO<sub>3</sub><sup>-</sup> anions.
- 13 • MgCO<sub>3</sub> dramatically lowers carbonate liquid density and increases compressibility.
- 14 • Assuming MgCO<sub>3</sub>-like structure, Fe-rich carbonatites remain buoyant in the mantle.

## 15 16 **Abstract**

17 MgCO<sub>3</sub> is one of the most important components of mantle-derived carbonatite melts, and  
18 yet also one of the most difficult to study experimentally. Attempts to constrain its thermodynamic  
19 properties are hampered by decarbonation, which occurs at only ~500 °C, far below its metastable  
20 1 bar melting temperature. Molecular dynamic simulations, however, can predict the  
21 thermodynamic properties of the MgCO<sub>3</sub> liquid component in spite of experimental challenges.  
22 Using the recently developed empirical potential model for high-pressure alkaline earth carbonate  
23 liquids (Hurt and Wolf 2018), we simulate melts in the MgCO<sub>3</sub>-CaCO<sub>3</sub>-SrCO<sub>3</sub>-BaCO<sub>3</sub> system  
24 from 773 to 2373 K up to 20 GPa. At 1 bar, MgCO<sub>3</sub> liquid assumes a novel topology characterized  
25 by a 4-fold coordination of the metal cation (Mg) with both the carbonate molecule and oxygen  
26 ion; this is distinct from the other alkaline earth carbonate liquids in which the metal cation is in  
27 ~6- and ~8-fold coordination with carbonate and oxygen. With increasing pressure, MgCO<sub>3</sub> liquid  
28 structure becomes progressively more like that of (Ca, Sr, Ba)CO<sub>3</sub> liquids with Mg<sup>2+</sup> approaching  
29 6-fold coordination with carbonate groups. The novel network topology of MgCO<sub>3</sub> liquid results  
30 in a melt that is significantly more buoyant and compressible than other alkaline earth carbonate  
31 liquids. Simulations of mixed MgCO<sub>3</sub>-bearing melts show that molar volume, compressibility,

32 enthalpy and heat capacity do not mix ideally with (Ca, Sr, Ba)CO<sub>3</sub> liquids at 1 bar, a consequence  
33 of preferential metal-cation ordering in MgCO<sub>3</sub>-bearing mixtures. As pressure increases, however,  
34 mixing progressively approaches ideality with respect to molar volume, becoming nearly ideal by  
35 12 GPa. The model is further applied to mantle-derived primary carbonatite melts with  
36 compositions, temperatures and pressures determined by published phase equilibrium  
37 experiments. The voluminous structure of liquid MgCO<sub>3</sub> results in a buoyant melt that inhibits a  
38 density crossover with the surrounding mantle. Assuming FeCO<sub>3</sub> liquid also adopts the same  
39 anomalous high-volume structure as MgCO<sub>3</sub>, we predict that even the most Fe-rich  
40 ferrocarbonatites would remain buoyant and be barred from sinking or stagnating in the mantle.

41

42 **Keywords:** MgCO<sub>3</sub> melt, carbonate liquid structure, carbonatite density, alkaline earth carbonates

43

44

## 1. Introduction

45 Carbonate plays an important role in partial melting of the mantle. It can lower the solidus  
46 of mantle peridotite and eclogite up to ~600 °C (e.g. Dasgupta and Hirschmann 2006; Dasgupta  
47 and Hirschmann 2007; Hammouda 2003), producing low degree partial melts of 0.03-0.3%  
48 carbonatite liquid (e.g. Green and Wallace 1988; Dalton and Wood 1993; Dasgupta and  
49 Hirschmann 2006). Carbonatite liquids are highly mobile owing to their ultralow viscosities (e.g.  
50 Kono et al. 2014). They are efficient agents of metasomatism (e.g. Green and Wallace 1988), are  
51 important for the petrogenesis of ocean island basalts (e.g. Dasgupta et al. 2006) and impact the  
52 deep carbon cycle (e.g. Dasgupta and Hirschmann 2010).

53 Of all the carbonate liquid components, MgCO<sub>3</sub> is one of the most geologically relevant.  
54 Carbonate enters the mantle through subduction of hydrothermally altered oceanic crust (e.g.  
55 Staudigel et al. 1989). Calcium from CaCO<sub>3</sub> partitions readily into the silicate phases of the mantle  
56 and is replaced by Mg, establishing MgCO<sub>3</sub> as a dominant carbonate mantle component  
57 (Biellmann et al. 1993). Investigations into the composition of primary carbonatite melts produced  
58 by partial melting of carbonated mantle eclogite and peridotite show that MgCO<sub>3</sub> along with  
59 CaCO<sub>3</sub> and FeCO<sub>3</sub> are the major components of interest (Dalton and Wood 1993; Dalton and  
60 Presnall 1998; Hammouda 2003; Ghosh et al 2009).

61 Carbonated mantle systems have been extensively studied via phase equilibrium  
62 experiments (e.g. Dalton and Wood 1993; Dalton and Presnall 1998; Hammouda 2003; Ghosh et

63 al 2009). While such experiments are immensely valuable, they have limitations. For example,  
64 small variations in the starting composition can result in marked changes to the location of the  
65 solidus in P-T space (Dasgupta and Hirschmann 2010). This is problematic given the significant  
66 compositional heterogeneity of carbonated mantle, both in its silicate and carbonate phases.  
67 Compositional complexity is further compounded by wide ranges of temperatures and pressures  
68 where partial melting may occur. Phase equilibrium experiments cannot be performed for every  
69 relevant composition, temperature and pressure. Furthermore, experimenters often adjust  
70 temperature and pressure together, making it difficult to disentangle temperature- and pressure-  
71 effects.

72 Thermodynamic models such as MELTS (Ghiorso et al. 2002) or THERMOCALC (Powell  
73 and Holland 1988) can help resolve these issues but they rely on knowledge of the standard state  
74 thermodynamic properties. For the most important carbonate crystal phases (e.g. magnesite,  
75 siderite and calcite), the standard state properties are well known (e.g. Berman et al. 1985).  
76 However, knowledge of the standard state thermodynamic properties of the respective liquids is  
77 limited because alkaline earth carbonates and  $\text{FeCO}_3$  decompose at temperatures lower than their  
78 1 bar melting temperatures. In spite of the difficulties posed by decarbonation, some properties of  
79 the  $\text{CaCO}_3$  component have been determined experimentally (e.g. Liu and Lange 2003; Hurt and  
80 Lange 2018; O’Leary et al 2015; Hurt 2018), but there is a near total absence of knowledge of the  
81 standard state thermodynamic properties of  $\text{MgCO}_3$  and  $\text{FeCO}_3$  liquid. This is due to the very low  
82 1 bar decarbonation temperatures (only  $500^\circ\text{C}$  for  $\text{MgCO}_3$ , Hurst 1991), which makes experiments  
83 on  $\text{MgCO}_3$ - and  $\text{FeCO}_3$ -bearing liquids nearly impossible at 1 bar.

84 At present, MD simulations provide the only plausible path for obtaining the complete set  
85 of carbonate liquid endmember properties needed to incorporate carbonate-silicate melting into a  
86 thermodynamic modeling framework like MELTS. The empirical potential model presented in  
87 Hurt and Wolf (2018) is designed specifically for simulations of alkaline earth carbonate liquids  
88 at mantle conditions. In this study, we apply that model to simulate liquids in the  $\text{MgCO}_3$ - $\text{CaCO}_3$ -  
89  $\text{SrCO}_3$ - $\text{BaCO}_3$  quaternary system from 773 to 2373 K up to 20 GPa. The simulations supply crucial  
90 constraints on the standard state thermodynamic properties of pure  $\text{MgCO}_3$  liquid which are  
91 difficult or impossible to determine experimentally.

92 Apart from endmember thermodynamic properties, the simulations explore liquid  
93 structure and mixing behavior in the  $\text{MgCO}_3$ - $\text{CaCO}_3$ - $\text{SrCO}_3$ - $\text{BaCO}_3$  quaternary system. The local

94 structure of carbonate liquids can be characterized by the coordination of the metal cations with  
95 neighboring oxygens and carbonate molecules. In the recent experimental studies of Hurt and  
96 Lange (2019) and Hurt (2018), the molar volume and compressibility of  $\text{MgCO}_3$  is estimated by  
97 systematic variations with the alkali and alkaline earth carbonates. Their estimates, however,  
98 depend on liquid structure, namely the coordination of  $\text{Mg}^{2+}$  with the carbonate groups. These  
99 coordination numbers, which are obtainable via MD simulations, are thus necessary for correctly  
100 interpreting the systematic trends in experimental density and compressibility measurements  
101 among alkali and alkaline earth carbonate liquids and will allow meaningful estimates of the  
102  $\text{MgCO}_3$  and  $\text{FeCO}_3$  liquid components to be made based on systematics.

103 To assess whether carbonate melts are buoyant throughout the upper mantle and transition  
104 zone, simulations are also performed on  $\text{CaCO}_3$ - $\text{MgCO}_3$  binary compositions from 1.5 to 20 GPa  
105 and 1423 to 1873 K along various pressure-temperature paths approximating that of subducting  
106 slabs. The simulation composition, temperature and pressure are representative of near-solidus  
107 carbonatite melts formed by low-degree partial melting of carbonated eclogite and peridotite. This  
108 is done in order to estimate the density of primary carbonatite melts as a function of depth and  
109 determine whether any compositions of carbonate melt are sufficiently dense to either stagnate  
110 upon initial melting or sink into the lower mantle. Given the likely similarity of  $\text{MgCO}_3$  and  $\text{FeCO}_3$   
111 liquid structures and volumes, we also explore the implications for ferrocarbonatite melts in the  
112 mantle.

## 113 2. Methods

114 For this study, we use a previously published empirical potential model for the simulation  
115 of alkaline earth carbonate liquids using rigid ions and partial charges. A complete derivation and  
116 assessment of this model is available in (Hurt and Wolf 2018) where it was also applied to the  
117 simulation of liquids in the  $\text{CaCO}_3$ - $\text{SrCO}_3$ - $\text{BaCO}_3$  system. This model is now applied to molecular  
118 dynamic (MD) simulations of  $\text{MgCO}_3$ -bearing liquids performed using the LAMMPS code  
119 (Plimpton, 1995).

120 42 different liquid compositions are simulated within the  $\text{MgCO}_3$ - $\text{CaCO}_3$ - $\text{SrCO}_3$ - $\text{BaCO}_3$   
121 quaternary over a temperature range of 773-2373 K and up to 20 GPa. MD simulations are  
122 performed with a timestep of 1 fs and total runtimes of 120 ps. Each simulation begins with an  
123 equilibration phase of 60 ps using the canonical (NVE) ensemble with the Berendsen barostat and  
124 thermostat (Berendsen et al., 1984), which equilibrates quickly and smoothly but deviates slightly

125 from the canonical ensemble. A second equilibration phase of 40 ps is performed under the NPT  
126 ensemble using the Nosé-Hoover barostats and thermostats (Nosé, 1984; Hoover, 1985). A third  
127 phase of 20 ps continues the NPT ensemble and constitutes the final production run.

128 Every simulation is checked to ensure that system energies and volumes have converged  
129 to within 0.02% and 0.27%, respectively. This level of volume convergence is achieved with a  
130 simulation size of 6860 atoms. Simulations are initialized with atomic positions and velocities  
131 corresponding to CaCO<sub>3</sub> liquid at 2.275 g/cm<sup>3</sup> density (equivalent to 1 bar pressure) and 1623 K.

### 132 **3. Results**

#### 133 ***3.1 Equation of state of MgCO<sub>3</sub> liquid***

134 Hurt and Wolf (2018) previously showed that CaCO<sub>3</sub>, SrCO<sub>3</sub> and BaCO<sub>3</sub> liquids have  
135 remarkably similar properties, with nearly parallel compression curves, 1 bar molar volumes that  
136 increase systematically with cation radius and congruent thermal expansion coefficients. Such  
137 systematic variation in molar volume and congruent thermal expansions, are corroborated by the  
138 experiments of Hurt and Lange (2019) and Hurt (2018).

139 To investigate whether the properties of MgCO<sub>3</sub> liquid follow the trends observed among  
140 CaCO<sub>3</sub>, SrCO<sub>3</sub> and BaCO<sub>3</sub>, the thermodynamic properties of MgCO<sub>3</sub> liquid have been calculated  
141 from the simulations (complete details and results are listed in Table A.1). Following Hurt and  
142 Wolf (2018), we attempt to fit the MgCO<sub>3</sub> simulation results with a temperature-dependent 3<sup>rd</sup>  
143 order Birch-Murnaghan equation of state (EOS), but the resulting models show a markedly poor  
144 fit to the data (Table 1). This is further exemplified by the large error bars on the fitted parameters.  
145 Unlike (Ca, Sr, Ba)CO<sub>3</sub> liquids, MgCO<sub>3</sub> liquid is highly compressible at pressures <2 GPa, and its  
146 rapid change in molar volume cannot be accommodated by a 3<sup>rd</sup> order Birch-Murnaghan, thus  
147 requiring us to adopt a 4<sup>th</sup> order Birch-Murnaghan EOS (details of the EOS are available in  
148 Appendix A).

149 The full set of fitted parameters for this EOS is given in Table 1. This 4<sup>th</sup> order Birch-  
150 Murnaghan EOS model recovers the simulated molar volumes in the 1100 – 2000 K temperature  
151 range up to 20 GPa with RMS volume residuals of 0.27 cm<sup>3</sup>/mol (0.81%). The 1100 K compression  
152 curve predicted by this best-fit EOS model is shown in Fig. 1 along with the raw simulated molar  
153 volume data as a function of pressure up to 12 GPa. The simulated compression curves of CaCO<sub>3</sub>,  
154 SrCO<sub>3</sub> and BaCO<sub>3</sub> liquids are also shown for comparison, together with the expected compression

155 behavior for MgCO<sub>3</sub> liquid (shown as a dotted line) assuming it follows the systematic trend of  
156 the other alkaline earth carbonates (discussed in detail below). Clearly, the model predicts a curve  
157 for MgCO<sub>3</sub> that is radically different from the other three alkaline earth carbonate components.  
158 The 1 bar molar volume is near that of SrCO<sub>3</sub> and decreases dramatically with pressure, implying  
159 a 1 bar compressibility far-exceeding that of the other alkaline earth carbonate liquids. The  
160 compression curve rapidly flattens out and at pressures > 5 GPa, where it begins to parallel the  
161 other alkaline earth carbonates. Liquids derive many of their thermophysical properties from their  
162 average atomic structure, and thus we explore the pressure-dependent atomic structure of MgCO<sub>3</sub>  
163 liquid to discover the root cause for its unique behavior among the alkaline-earth carbonates.

### 164 **3.2 Distinct structure of MgCO<sub>3</sub> liquid**

165 Though liquids lack long-range order, they do possess a short-range order that can be  
166 described using a pair distribution function (pdf). For a particular pair of atomic types (*i* and *j*),  
167 pdf curves give the average density of *j* as a function of distance from *i*. Liquid structure can also  
168 be described by coordination numbers for a given atomic pair. Average coordination numbers are  
169 calculated as weighted averages of the pdf curves,  $g_{ij}(r)$ :

$$CN_{ij} = 4\pi \int_0^{r_1} r^2 g_{ij}(r) \rho_j dr \quad \text{Eq. 1}$$

170 where  $r$  is the atomic separation distance,  $\rho_j$  is the average atomic number density of atom *j*, and  
171  $r_1$  is the maximum cutoff radius located at the first minimum in the PDF, representing the outer  
172 boundary of the first nearest-neighbor peak.

173 Hurt and Wolf (2018) used the same empirical potential model to simulate (Ca, Sr, Ba)CO<sub>3</sub>  
174 liquids, and demonstrated that they have remarkably similar liquid structures and coordination  
175 numbers for the metal-oxygen (M-O), carbon-carbon (C-C) and metal-carbon (M-C) pairs. At  
176 ambient pressure, C-C and M-C coordination numbers are the same for each liquid at 10.9 and 5.9  
177 respectively. M-O coordination numbers are similar for the three endmember liquids, increasing  
178 systematically from Ca to Ba (Ca-O: 6.9, Sr-O: 7.3 and Ba-O: 7.7).

179 Based on the new simulations performed in this study, we analyze the structure of MgCO<sub>3</sub>  
180 liquid. The 1 bar results are summarized in Fig. 2, which shows a distinctly different atomic  
181 structure and coordination environment for MgCO<sub>3</sub> as compared to the other alkaline earth  
182 carbonate liquids, visible in terms of C-C, M-O and M-C pairs. At 1 bar, the Mg-O and Mg-C

183 coordination is tetrahedral (4), while the C-C coordination (11.6) is nearly ideal closest-packing,  
184 compared to CaCO<sub>3</sub>-SrCO<sub>3</sub>-BaCO<sub>3</sub> liquids (10.9). The most significant of these differences is that  
185 the M-C coordination, which is consistently 6 for the other alkaline earth carbonate liquids, is only  
186 4 for MgCO<sub>3</sub>—the same as in alkali carbonates (e.g. Roest et al 2017).

187 To determine whether the unique structure of MgCO<sub>3</sub> liquid persists at high pressure,  
188 isothermal compression simulations are analyzed at 1100 K between 1 bar and 12 GPa. M-C and  
189 M-O coordination numbers are calculated at each pressure and shown in Fig. 3. As pressure  
190 increases, the Mg-O coordination number increases linearly from 4 (at 1 bar) to 5.6 (at 12 GPa).  
191 In the high-pressure regime, M-O coordination number adopts systematic behavior among the  
192 alkaline earth carbonates: the coordination number is ~10 for Ba-O, ~9 for Sr-O, ~8 for Ca-O and  
193 ~6 for Mg-O. Thus, at pressure, the Mg-O coordination number is consistent with what might be  
194 expected from periodic table systematics. For the M-C coordination numbers, CaCO<sub>3</sub>-SrCO<sub>3</sub>-  
195 BaCO<sub>3</sub> liquids average around 6 at 1 bar and then increase modestly to ~6.8 by 12 GPa. The Mg-  
196 C coordination starts off at 4 at 1 bar and converges rapidly to values consistent with the other  
197 alkaline earth carbonates. Thus, simulations indicate that the liquid structure of MgCO<sub>3</sub> becomes  
198 progressively more like that of the other alkaline earth carbonates with compression, becoming  
199 nearly indistinguishable by 12 GPa.

### 200 **3.3 Non-ideal mixing for MgCO<sub>3</sub> liquid at low pressure**

201 Hurt and Wolf (2018) simulated alkaline earth carbonate liquids in three binary systems:  
202 CaCO<sub>3</sub>-SrCO<sub>3</sub>, CaCO<sub>3</sub>-BaCO<sub>3</sub> and SrCO<sub>3</sub>-BaCO<sub>3</sub>. It was found that molar volumes and molar  
203 isobaric heat capacities and compressibility all mix ideally across a wide range of temperatures  
204 and pressures. To test whether such ideal mixing behavior extends to MgCO<sub>3</sub>-bearing liquids,  
205 simulations of mixed liquids are performed in the MgCO<sub>3</sub>-CaCO<sub>3</sub>-SrCO<sub>3</sub>-BaCO<sub>3</sub> quaternary  
206 system at 1 bar and 1100 K. For any property of interest, we define the mixing quantity as the  
207 deviation from a compositionally-weighted average of the endmembers:

$$\Delta Z_{mix} = Z - \sum Z_i X_i \quad \text{Eq. 2}$$

208 where  $Z$  is the molar quantity of interest (like volume or enthalpy) for the liquid mixture,  $X_i$  is mol  
209 fraction of each endmember, and  $Z_i$  is the quantity for each pure endmember at the specified  
210 temperature and pressure. The ideality of mixing in terms of both volume and enthalpy is assessed

211 for simulated Mg-carbonate binaries and visualized in Fig. 4 (with direct simulation results  
212 reported in Appendix Table C.2).

213 Properties determined from MD simulations always contain uncertainties due to random  
214 Afluctuations and system size limitations. We can reduce the effects of this noise and better  
215 characterize non-ideal mixing by fitting a simple sub-regular mixing model to the simulated  $\Delta V_{mix}$   
216 and  $\Delta H_{mix}$  values:

$$\Delta Z_{mix} = \left( w + \Delta w \left[ X - \frac{1}{2} \right] \right) \cdot X[1 - X] \quad \text{Eq. 3}$$

217 where  $\Delta Z_{mix}$  is the mixing property for either volume or enthalpy,  $X$  is mol fraction of  $\text{MgCO}_3$ ,  
218 and  $w$  and  $\Delta w$  are constants which have been fitted using least squares minimization. The best-fit  
219 values of  $w$  and  $\Delta w$  at 1100 K and 1 bar for all three binaries are given in Appendix Table C.3.  
220 Fig. 4 depicts  $\Delta V_{mix}$  in panel a and  $\Delta H_{mix}$  in panel b for each simulated mixture as a function of  
221  $\text{MgCO}_3$  content along with the best-fit sub-regular solution model (Eq. 3). Note that, for  $\Delta H_{mix}$ ,  
222 simulated total energy values are used instead of enthalpy because they are equal at 1 bar and  
223 because simulated enthalpy has larger errors than total energy due to fact that enthalpy calculations  
224 fold in fluctuations on both pressure and volume. Fig. 4a shows significant non-ideal volume of  
225 mixing for all binaries, especially along the  $\text{CaCO}_3$ - $\text{MgCO}_3$  binary where  $\Delta V_{mix}$  is as large as -  
226  $0.87 \pm .11 \text{ cm}^3/\text{mol}$ . Volumes of mixing are nearly all predicted to be negative. For all binaries,  
227 the mixing behavior is slightly asymmetric; the magnitude of  $\Delta V_{mix}$  reaches a maximum at 60-75  
228 mol %  $\text{MgCO}_3$ . The non-ideal mixing of volumes in  $\text{MgCO}_3$ -bearing liquids means that volumetric  
229 derivative properties such as compressibility also cannot mix ideally.

230 The case of enthalpy of mixing ( $\Delta H_{mix}$ ) is closely analogous. Unlike liquids in the  $\text{CaCO}_3$ -  
231  $\text{SrCO}_3$ - $\text{BaCO}_3$  system, enthalpy does not mix ideally among  $\text{MgCO}_3$ -bearing mixtures. Fig. 4b  
232 shows that  $\Delta H_{mix}$  is uniformly negative or statistically consistent with zero across the binary for  
233 every mixture. The peak magnitude of  $\Delta H_{mix}$  increases systematically from  $\text{CaCO}_3$  (31 KJ/mol)  
234 to  $\text{BaCO}_3$  (~12 KJ/mol). Within each binary, the magnitude of  $\Delta H_{mix}$  peaks at 60-75 mol%  
235  $\text{MgCO}_3$ . Interestingly, the  $\text{BaCO}_3$ - $\text{MgCO}_3$  system exhibits the lowest  $\Delta V_{mix}$  but the highest  
236  $\Delta H_{mix}$ ; this suggests that the mechanism responsible for non-ideal mixing in volumetric properties  
237 is not the same as the one driving non-ideal mixing in enthalpic properties.

238 Hurt and Wolf (2018) found that simulations predict isobaric heat capacities to mix ideally  
239 according to mol fraction in  $\text{CaCO}_3$ - $\text{SrCO}_3$ - $\text{BaCO}_3$  liquids. Simulations in this study of  $\text{MgCO}_3$ -



240 bearing binary liquids from 1100 to 2000 K enabled calculation of the isobaric 1 bar heat capacity.  
241 For  $\text{CaMg}(\text{CO}_3)_2$ ,  $\text{SrMg}(\text{CO}_3)_2$  and  $\text{BaMg}(\text{CO}_3)_2$ , the heat capacity is estimated to be 146, 140 and  
242 139 J/mol, which are lower than their ideal values by 7%, 11%, and 9%, respectively. Heat  
243 capacities are thus systematically lower (9% on average) than expected for  $\text{MgCO}_3$ -bearing-  
244 systems.

### 245 ***3.4 Structural ordering and non-ideality in $\text{MgCO}_3$ mixtures***

246 As noted above, liquid properties (e.g. molar volume, compressibility, enthalpy and heat  
247 capacity) do not mix ideally in the  $\text{MgCO}_3$ -binary compositions as they do in the  $\text{CaCO}_3$ - $\text{SrCO}_3$ -  
248  $\text{BaCO}_3$  liquid system at 1 bar. The non-ideal source of this mixing should likely manifest as some  
249 structural anomaly evident in the pdf curves of mixtures (i.e. there should be some noticeable  
250 difference between the pdf curves of pure  $\text{MgCO}_3$  compared to an  $\text{MgCO}_3$ -bearing mixture). Such  
251 a difference might help reveal the mechanism driving non-ideal mixing behavior.

252 Within the  $\text{MgCO}_3$ - $\text{CaCO}_3$ - $\text{SrCO}_3$ - $\text{BaCO}_3$  quaternary there are six binaries. Various  
253 compositions within each binary were simulated at 1100 K and 1 bar and pdf curves were  
254 calculated for every atomic pair. The full range of pdf curves for M-O, M-C and C-C pairs for each  
255 binary composition is available in Appendix Fig. C.1. The striking uniformity of pdf curves  
256 demonstrates that M-O, M-C and C-C pairs in binary liquids retain the same structure and  
257 coordination as in the pure liquids. This means that, at 1 bar,  $\text{Mg}^{2+}$  maintains its 4-fold coordination  
258 with carbonate and oxygen independent of bulk composition. Similarly, if small amounts of  
259  $\text{CaCO}_3$ ,  $\text{SrCO}_3$  and  $\text{BaCO}_3$  are mixed into  $\text{MgCO}_3$  liquid,  $\text{Ca}^{2+}$ ,  $\text{Sr}^{2+}$  and  $\text{Ba}^{2+}$  ions maintain their  
260 octahedral coordination with carbonate. While the Mg-O and Mg-C coordination in mixtures is  
261 the same as in pure  $\text{MgCO}_3$  liquid (i.e.  $\text{Mg}^{2+}$  maintains a coordination of 4 with carbonate and  
262 oxygen atoms) there are some notable differences between the pdf curves of pure and mixed  
263  $\text{MgCO}_3$ .

264 Simulations reveal that the key structural difference between pure and mixed  $\text{MgCO}_3$   
265 liquids is metal cation ordering. In pure  $\text{MgCO}_3$  liquid at 1 bar, the primary Mg-Mg coordination  
266 shell is actually composed of two partially overlapping shells. The inner shell contains 3 Mg atoms  
267 at an average distance of 3.7 Å, and the outer shell has an additional 9 Mg atoms at an average  
268 distance of 5.3 Å. When  $\text{MgCO}_3$  is mixed with another carbonate, this primary coordination shell  
269 is split, with the inner shell preferentially filled by other metal cations. Figure 5 shows the Mg-Mg  
270 and Mg-Ca pdf curves in pure  $\text{MgCO}_3$  and  $\text{MgCa}(\text{CO}_3)_2$ ; these curves show that  $\text{Mg}^{2+}$  vacates the

271 inner coordination shell in mixed compounds and is replaced by  $\text{Ca}^{2+}$ . This kind of cation ordering  
272 was not observed in  $\text{CaCO}_3$ - $\text{SrCO}_3$ - $\text{BaCO}_3$  liquids. Such ordering in  $\text{MgCO}_3$ -bearing mixtures can  
273 explain why some properties of  $\text{MgCO}_3$ -bearing liquids do not mix ideally, while  $\text{CaCO}_3$ - $\text{SrCO}_3$ -  
274  $\text{BaCO}_3$  liquids do. This behavior is likely related to cation ordering in the calcite-dolomite-  
275 magnesite series, which produces the highly ordered dolomite structure, where cations of mixed  
276 sizes are accommodated with minimal lattice strain (Vinograd 2006). Given that  $V_{mix}$  is found to  
277 be either negative or insignificant, cation ordering likely allows the liquid to pack space more  
278 efficiently for liquid Mg-carbonate mixtures.

### 279 ***3.5 Ideal mixing of $\text{MgCO}_3$ liquid at high pressure***

280         Though its structure and compressive properties are distinct at low pressures,  $\text{MgCO}_3$   
281 liquid increasingly resembles other alkaline earth carbonates at higher pressures. This is apparent  
282 in the compression curves, which become nearly parallel between 5 and 10 GPa as shown in Fig. 1.  
283 To further investigate, binary mixture simulations of  $\text{CaMg}(\text{CO}_3)_2$ ,  $\text{SrMg}(\text{CO}_3)_2$  and  $\text{BaMg}(\text{CO}_3)_2$   
284 are also performed at 1100 K up to 12 GPa, assessing whether volumes and enthalpies mix ideally  
285 at pressure. The values of  $\Delta V_{mix}$  calculated from the resulting simulations are  $-0.02 \pm .03$ ,  $-0.13 \pm$   
286  $.03$  and  $-0.11 \pm .03$   $\text{cm}^3/\text{mol}$  for  $\text{CaMg}(\text{CO}_3)_2$ ,  $\text{SrMg}(\text{CO}_3)_2$  and  $\text{BaMg}(\text{CO}_3)_2$  respectively. These  
287  $\Delta V_{mix}$  values are dramatically smaller than at 1 bar (which range between  $-0.34$  and  $-0.91$   $\text{cm}^3/\text{mol}$ ).  
288 Fig. 6 shows the compression behavior of  $\Delta V_{mix}$  at 1100 K, normalized to the pressure-dependent  
289 absolute volume difference between  $\text{CaCO}_3$  and  $\text{MgCO}_3$  liquid,  $\Delta V_{\text{MgCO}_3\text{-CaCO}_3}$ . This pressure-  
290 dependent normalization is necessary since the molar volume of the  $\text{MgCO}_3$ - $\text{CaCO}_3$  binary  
291 mixture falls between the volumes of the pure endmembers, and thus at pressures where pure  
292  $\text{CaCO}_3$  and  $\text{MgCO}_3$  volumes converge,  $\Delta V_{mix}$  will appear small; normalizing to the volume  
293 difference between the endmembers corrects for this. As seen in the figure,  $\Delta V_{mix}$  approaches 0 as  
294 pressure increases, reflecting increasingly ideal mixing.

295         At low pressures, it was previously shown that metal-cation ordering provides a  
296 mechanistic explanation for non-ideal mixing of at least some of the properties in  $\text{MgCO}_3$ -bearing  
297 liquids. Since  $\Delta V_{mix}$  diminishes to nearly 0 at 12 GPa, we might expect to see little difference  
298 between Mg-Mg pdf curves in pure  $\text{MgCO}_3$  versus  $\text{MgCO}_3$  mixtures at that pressure. The inset on  
299 Figure 6 shows, in fact, that the structural difference between pure and mixed  $\text{MgCO}_3$  liquids

300 progressively lessens with pressure (up to 12 GPa), supporting the notion that metal cation ordering  
301 correctly explains non-ideal mixing in volumetric properties among  $\text{MgCO}_3$ -bearing liquids.

302 In contrast, the simulations indicate that non-ideal mixing of enthalpy does not disappear  
303 at high pressure like  $\Delta V_{mix}$ . At 12 GPa,  $\Delta H_{mix}$  for  $\text{CaMg}(\text{CO}_3)_2$ ,  $\text{SrMg}(\text{CO}_3)_2$  and  $\text{BaMg}(\text{CO}_3)_2$  is  
304 calculated to be -2.9, -8.2 and -11.7 kJ/mol respectively. Normalizing  $\Delta H_{mix}$  to the difference in  
305 enthalpy between the endmembers would yield a more meaningful comparison (since absolute  
306 values of enthalpy increase with pressure). This result gives a normalized  $\Delta H_{mix}$  of -1.2, -2.1 and -  
307 1.9% at 12 GPa compared to -1.1, -1.8 and -4.5% at 1 bar for  $\text{CaMg}(\text{CO}_3)_2$ ,  $\text{SrMg}(\text{CO}_3)_2$  and  
308  $\text{BaMg}(\text{CO}_3)_2$ , respectively.  $\text{BaMg}(\text{CO}_3)_2$  is the only mixture that undergoes a significant reduction  
309 in  $\Delta H_{mix}$  with pressure, while the normalized  $\Delta H_{mix}$  for the other binary liquids remain unchanged.  
310 This suggests that cation ordering in  $\text{MgCO}_3$ -bearing liquids is not solely responsible for non-ideal  
311 mixing of enthalpies.

## 312 4. Discussion

### 313 4.1 Fourfold cation coordination in $\text{MgCO}_3$ liquid at 1 bar

314 Previous molecular dynamic studies have found that most alkaline earth carbonate liquids  
315 ( $\text{CaCO}_3$ ,  $\text{SrCO}_3$ ,  $\text{BaCO}_3$ ) adopt similar 1 bar atomic structures, with metal cations in octahedral  
316 coordination with carbonate anions and 7-8 fold coordination with oxygen (Hurt 2018, Vuilleumier  
317 2014). A thorough search of the literature reveals, to the best of our knowledge, that this study is  
318 the first to demonstrate that  $\text{MgCO}_3$ -bearing melts are unique among those of the alkaline earth  
319 carbonates, with  $\text{Mg}^{2+}$  in tetrahedral coordination with both oxygen and carbonate anions. This  
320 structural anomaly is all the more surprising, given that Mg-bearing carbonate crystals (magnesite,  
321 dolomite, huntite, and northsite) all possess 6-fold oxygen coordination.

322 In silicate systems,  $\text{Mg}^{2+}$  is known to enter into 4-fold coordination with oxygen in glasses  
323 and melts across a wide range of compositions (e.g. Roy 1950; Waseda and Toguri 1977; Kubicki  
324 et al 1992; Shimodo et al 2008; Trcera et al 2009; Cormier and Cuello 2013; Morizet et al 2017).  
325 In silicate crystals,  $\text{Mg}^{2+}$  is mostly in 6-fold coordination; however, two silicate crystal phases,  
326 spinel and åkermanite ( $\text{Ca}_2\text{Mg}[\text{Si}_2\text{O}_7]$ ), host  $\text{Mg}^{2+}$  in fourfold coordination (e.g. Kroecker and  
327 Stebbins 2000). Thus, while  $\text{Mg}^{2+}$  is mostly found in 6-fold coordination in solid silicate phases,  
328 it commonly enters into 4-fold coordination upon fusion, opening the door for similar behavior in  
329 carbonate systems.

330 Unfortunately, it is difficult to assess the coordination of  $\text{Mg}^{2+}$  in carbonate melts from past  
331 analytical studies. Detailed structural information on  $\text{Mg}^{2+}$  coordination in  $\text{MgCO}_3$ -bearing  
332 carbonate melts/glasses is largely unavailable. This is in part because melt structure is commonly  
333 determined via experimental analyses (such as XANES or EXAF) of glasses, and while silicate  
334 melts readily quench to glass, there is only one entirely carbonate system that is capable of  
335 vitrification:  $\text{K}_2\text{CO}_3$ - $\text{MgCO}_3$  (e.g. Datta et al 1964; Ragone et al 1966). This system is doubly  
336 unique because it is the only known  $\text{MgCO}_3$ -bearing carbonate liquid that forms a stable melt at 1  
337 bar (Ragone et al 1966).  $\text{K}_2\text{CO}_3$ - $\text{MgCO}_3$  glass structures have been studied by both infrared (Datta  
338 et al 1964; Genge et al 1995) and Raman spectroscopy (Sharma and Simons 1980; Genge et al  
339 1995). Neither Genge nor Sharma comment on  $\text{Mg}^{2+}$  coordination in their spectroscopic studies.  
340 However, Datta et al (1964) posited that the low refractive index and density of the  $\text{K}_2\text{CO}_3$ - $\text{MgCO}_3$   
341 glass (compared to the respective crystals) may result from a low (4-fold) Mg coordination. Datta  
342 also recognized the significance of the fact that the only known  $\text{MgCO}_3$ -bearing carbonate liquid  
343 that is stable at 1 bar is also the only carbonate capable of quenching to a glass, implying its  
344 structure must somehow be unique among alkaline earth carbonate liquids; Datta thus  
345 hypothesized that it could be related to a decrease in  $\text{Mg}^{2+}$  coordination number. Our MD  
346 simulations suggest that  $\text{MgCO}_3$  liquid does in fact assume a unique topology characterized by a  
347 low (4-fold) coordination of  $\text{Mg}^{2+}$ , which corroborates the suppositions of Datta et al. (1964) on  
348 the structure of  $\text{MgCO}_3$ -bearing carbonate melts.

#### 349 ***4.2 Comparison of $\text{MgCO}_3$ to other alkaline earth carbonate liquids***

350 From the simulations of this study, it appears that  $\text{MgCO}_3$  has a liquid structure that is  
351 distinct from the other alkaline earth carbonates and properties that deviate strongly from those  
352 predicted on the basis of systematic variations (see Hurt 2018; Hurt and Lange 2019). Hurt and  
353 Lange (2019) explored systematic variations in the 1 bar molar volumes of alkali and alkaline earth  
354 carbonate liquids. On the basis of systematic trends, two different estimates of  $\text{MgCO}_3$  liquid molar  
355 volume were made; one estimate assumes that  $\text{Mg}^{2+}$  is in 6-fold coordination with carbonate and  
356 oxygen and has a liquid structure that is like the other alkaline earth carbonates. The other estimate,  
357 based on preliminary results from this study, assumes  $\text{Mg}^{2+}$  is in 4-fold coordination with oxygen  
358 and carbonate and has a liquid structure that is more like an alkali carbonate. Under the 6-fold  
359 assumption, Hurt and Lange predict a 1 bar  $\text{MgCO}_3$  liquid molar volume of  $34.4 \pm .6 \text{ cm}^3/\text{mol}$ . In

360 the case of a 4-fold Mg-O coordination, Hurt and Lange (2019) estimated that MgCO<sub>3</sub> would have  
361 a 1 bar liquid molar volume of ~40 cm<sup>3</sup>/mol at 1100 K.

362 Our simulations clearly predict 4-fold coordination for Mg<sup>2+</sup> and a liquid structure that is  
363 more like alkali carbonate than typical alkaline earth carbonates (a full discussion of similarities  
364 between MgCO<sub>3</sub> and alkali carbonate liquid structure is available in Appendix B). In accordance  
365 with the estimates of Hurt and Lange (2019), our simulations predict a larger 1 bar molar volume  
366 than what might be expected from systematic variations in the molar volumes of alkaline earth  
367 carbonate liquids. The fitted Birch-Murnaghan EOS model (Appendix Eq. A.1-A.4) predicts a 1  
368 bar MgCO<sub>3</sub> liquid volume of 44.21±.09 cm<sup>3</sup>/mol at 1100 K. However, it's likely that the actual  
369 volume is somewhat lower since the empirical potential model of Hurt and Wolf (2018) typically  
370 slightly overestimates 1 bar volumes. For CaCO<sub>3</sub>, SrCO<sub>3</sub> and BaCO<sub>3</sub> liquids, the model requires a  
371 -0.35, -0.33 and -0.75 GPa pressure correction, respectively, to bring simulated 1 bar volumes into  
372 agreement with the experimental projections of Hurt and Lange (2019). An analogous -0.6 GPa  
373 pressure correction would bring the MgCO<sub>3</sub> simulations into agreement with the alkali-like  
374 structural predictions from Hurt and Lange (2019).

375 Hurt (2018), provides analogous systematic trend equations for the compressibility of  
376 alkali and alkaline earth carbonate liquids based on a positive linear relationship between liquid  
377 compressibility and volume of fusion. Their model equation predicts a compressibility for MgCO<sub>3</sub>  
378 liquid at 1100 K of ~23±1 10<sup>-2</sup> GPa<sup>-1</sup> assuming it fits into the alkali carbonate trend and ~18±6 10<sup>-2</sup>  
379 GPa<sup>-1</sup> if it fits into the alkaline-earth trend. Given the similarity of the MgCO<sub>3</sub> liquid structure to  
380 Li<sub>2</sub>CO<sub>3</sub> (Appendix Fig. B.1), the alkali carbonate trend might actually provide a better prediction  
381 (for more details regarding similarities between MgCO<sub>3</sub> and alkali carbonates, see Appendix B).  
382 These estimates of MgCO<sub>3</sub> liquid compressibility differ dramatically from other alkaline earth  
383 carbonate liquids (i.e. CaCO<sub>3</sub>, SrCO<sub>3</sub> and BaCO<sub>3</sub>) which have relatively modest 1 bar/1100 K  
384 compressibilities of 4.33 - 5.97 · 10<sup>-2</sup> GPa<sup>-1</sup>. Our MgCO<sub>3</sub> liquid simulations predict a bulk modulus  
385 (K<sub>T</sub>) of 6.15±.15 GPa, which is equivalent to a compressibility ( $\beta_T$ ) of 16.3 · 10<sup>-2</sup> GPa<sup>-1</sup> at 1100 K,  
386 broadly consistent with the elevated values predicted by Hurt (2018).

### 387 ***4.3 Comparison to previous thermodynamic studies of MgCO<sub>3</sub> liquid properties***

388 As noted above, the structure of MgCO<sub>3</sub> liquid becomes more like the other alkaline earth  
389 carbonates as it is subjected to progressively higher pressures. By 12 GPa, the M-O and M-C  
390 coordination numbers of MgCO<sub>3</sub> liquid converge to values in line with CaCO<sub>3</sub>, SrCO<sub>3</sub>, and BaCO<sub>3</sub>

391 liquid (Fig. 2). This pressure-induced transformation of liquid structure is also evident in the  
392 compression curve of MgCO<sub>3</sub> liquid, which begins to parallel the other three alkaline earth  
393 carbonate liquids at 5-10 GPa (Fig. 1).

394 Our predictions of the standard state thermodynamic properties of MgCO<sub>3</sub> liquid stand in  
395 stark contrast to previous estimates made by Kang et al. 2016. These calculations fit a  
396 thermodynamic model to the congruent melting curve of MgCO<sub>3</sub>, which is bracketed by four  
397 experimentally determined points (~1858 K at 3 GPa & 1883 K at 3.6 GPa from Irving and Wyllie  
398 1975, and 2183 K at 8 GPa & 2363 K at 15 GPa from Katsura and Ito 1990). This approach arrives  
399 at a molar volume of MgCO<sub>3</sub> liquid of ~32 cm<sup>3</sup>/mol and a compressibility of  $2.6 \cdot 10^{-2}$  GPa<sup>-1</sup> at  
400 1100 K and 1 bar. While the MgCO<sub>3</sub> properties proposed by Kang et al. differ markedly from our  
401 simulation results, Kang et al. arrived at their values using a method that is statistically  
402 problematic. The estimates of standard state thermodynamic properties of MgCO<sub>3</sub> liquid (and  
403 FeCO<sub>3</sub> as well) proposed by Kang et al. were calculated by fusion curve analysis. The fusion curve  
404 of MgCO<sub>3</sub> is currently bracketed by 4 experimental points (and only 3 for FeCO<sub>3</sub>). However, 5  
405 thermodynamic parameters are fitted based on only 4 experimental observations. Since the number  
406 of fitted parameters exceeds the number of constraining observations, the reported thermodynamic  
407 solution is highly under-constrained and non-unique, allowing alternative sets of thermodynamic  
408 properties to recover the observables just as well.

409 We can see some of the resulting issues directly in the fitted thermodynamic properties  
410 proposed by Kang et al. (2016); for example, the thermal expansions of MgCO<sub>3</sub> and FeCO<sub>3</sub> liquid  
411 are identical to the thermal expansion of their respective crystal phases. The thermal expansion of  
412 a liquid is generally expected to be substantially greater than that of the crystal, however (e.g.  
413 Lange 1997). CaCO<sub>3</sub>, SrCO<sub>3</sub> and BaCO<sub>3</sub> liquids, for example, have a thermal expansion ~3 times  
414 greater than their respective crystal phases (Hurt and Lange 2018). Kang et al. also give a  
415 temperature dependence of compressibility ( $\delta\beta_T/\delta T$ ) of MgCO<sub>3</sub> liquid that is lower, by an order of  
416 magnitude, than those of CaCO<sub>3</sub>, SrCO<sub>3</sub> and BaCO<sub>3</sub> liquids (Hurt et al. 2018). For these reasons,  
417 we strongly recommend the standard state MgCO<sub>3</sub> liquid thermodynamic properties derived from  
418 this study.

#### 419 ***4.4 The density of primary carbonatite melts***

420 Natural carbonatite liquids have been shown to be effective agents of mantle metasomatism  
421 and scavengers of trace elements (e.g. Blundy and Dalton 2000), and thus the mobility and ascent

422 rates of primary carbonatite melts are particularly geologically important. Ascent rate depends  
423 mostly on melt viscosity and density contrast. Viscosity has been measured at temperatures and  
424 pressure representative of the mantle for calcitic and dolomitic liquids (e.g. Kono et al. 2014). The  
425 densities of some important carbonate liquid components (e.g.  $\text{CaCO}_3$ ) at pressure have been  
426 constrained by 1 bar liquid density experiments (e.g. Liu and Lange 2003; Hurt and Lange 2018)  
427 and liquid sound speed measurements (e.g. O’Leary et al. 2015; Hurt 2018) as well as by molecular  
428 dynamic simulations (e.g. Vuilleumier et al 2014). However, primary carbonatite melts generated  
429 in the mantle by low-degree partial melting contain significant amounts of  $\text{MgCO}_3$  and  $\text{FeCO}_3$   
430 (Dalton and Wood 1993; Dalton and Presnall 1998; Ghosh et al. 2009).

431 While the densities of primary carbonatite melts along a carbonated mantle liquidus are  
432 mostly unknown, it may be estimated by simulations from this study. Using the compositions of  
433 low-degree primary carbonatite melts generated in phase equilibrium experiments of carbonated  
434 peridotite and eclogite (Dalton and Wood 1993; Dalton and Presnall 1998; Hammouda 2003;  
435 Ghosh et al. 2009), simulations at temperature and pressure are performed for simplified  
436 experimental compositions by projecting them into the  $\text{CaCO}_3$ - $\text{MgCO}_3$  binary. Complete details  
437 on these calculations are available in Appendix D.

438 The simulated density results are listed in Table 2 and depicted as a function of depth in  
439 Fig. 7. The simulations indicate that  $\text{CaCO}_3$ - $\text{MgCO}_3$  binary liquids will be relatively low in density  
440 due to the open network topology of the  $\text{MgCO}_3$  melt component. Thus, primary carbonatite melts  
441 maintain a significant density contrast with the surrounding mantle rocks throughout the entire  
442 upper mantle and transition zone. Even the densities of melts from Hammouda (2003), which  
443 represent a cold slab subduction PT path (and are relatively enriched in denser  $\text{CaCO}_3$  and  $\text{FeCO}_3$   
444 components) never approach that of the mantle. Given the ultralow viscosity of these kinds of  
445 liquids, any positive density contrast will swiftly drive liquid ascent; any degree of carbonate melt  
446 will thus quickly escape from a descending slab, inhibiting the subduction and storage of carbonate  
447 into the lower mantle.

448 The only common carbonate component heavy enough to potentially affect a density  
449 crossover in the mantle is  $\text{FeCO}_3$  (which is a common component in mantle-derived carbonatite  
450 melts, e.g. Hammouda 2003). Though our work does not directly address iron partitioning in  
451 carbonate-rich melts, we can use our model to approximate a minimum threshold iron-content that  
452 a hypothetical ferrocarnatite must contain in order to affect a density crossover within the

453 mantle. While FeCO<sub>3</sub> liquid was not directly simulated in this study, it's likely that FeCO<sub>3</sub> shares  
 454 the volumetric properties of MgCO<sub>3</sub>, since Fe<sup>2+</sup> and Mg<sup>2+</sup> have the same valence and similar ionic  
 455 radii, and thus can frequently occupy the same atomic sites within crystal lattices and liquid  
 456 pseudo-lattices. Assuming that MgCO<sub>3</sub> liquid molar volume is a reasonable proxy for FeCO<sub>3</sub>, the  
 457 FeCO<sub>3</sub> concentration necessary for affecting a density crossover can be calculated as a function of  
 458 depth for a ferrocarbonatite in the MgCO<sub>3</sub>-CaCO<sub>3</sub>-FeCO<sub>3</sub> system. For the purposes of this  
 459 calculation, it will be assumed that the molar volumes of all three components mix ideally and that  
 460  $X^{Mg} = X^{Ca}$ . The MgCO<sub>3</sub> & FeCO<sub>3</sub> liquid volumes are approximated at temperature and pressure  
 461 using the thermodynamic properties presented this study (Table 1) in conjunction with Eqs. A.1-  
 462 A.4. The partial molar volume of the CaCO<sub>3</sub> liquid component is accurately estimated by  
 463 combining experimental and theoretical constraints, using a 3<sup>rd</sup> order Birch-Murnaghan EOS with  
 464 properties taken from the 1 bar molar volume model of Hurt and Lange (2019), the compressibility  
 465 results of Hurt (2018) and the  $K'$  results from Hurt and Wolf (2018). The partial molar volume of  
 466 the MgCO<sub>3</sub>, FeCO<sub>3</sub> and CaCO<sub>3</sub> components were calculated at P-T conditions along an average  
 467 carbonated peridotite solidus given by Dasgupta and Hirschmann (2010):

$$T(^{\circ}C) = 0.0238 \times P^3 - 2.2084 \times P^2 + 73.7991 \times P + 830.3808 \quad \text{Eq. 4}$$

468 where P is in GPa. Using this approach, Fig. 8a shows the minimum requisite FeCO<sub>3</sub> concentration  
 469 needed for a ferrocarbonatite to stagnate in the mantle gradually decreases through the upper  
 470 mantle from a mol fraction of ~1 in the crust, to 0.5 (35 wt.% FeO) at the top of the transition zone.  
 471 Throughout the transition zone, the threshold iron content is ~0.65 mol fraction FeCO<sub>3</sub>. Such iron  
 472 concentrations far exceed what's observed in phase equilibrium experiments on carbonated  
 473 peridotite/eclogite (which generally produce carbonatite melts with <10 wt. % FeO). Fig. 8b shows  
 474 the density of a melt with an approximate composition of a natural ferrocarbonatite (Thompson et  
 475 al. 2002) which was calculated as a function of depth using the technique described above. As  
 476 evident, its density remains consistently lower than the mantle through the transition zone.

477 It's difficult to assess whether significant volumes of such highly Fe-enriched (>40 mol%  
 478 FeCO<sub>3</sub>) ferrocarbonatites are actually produced in the mantle. After an exhaustive search of the  
 479 literature, the ferrocarbonatite in Swartbooisdrif, Namibia (Thompson et al. 2002) appears to be  
 480 the only natural ferrocarbonatite yet identified with an unambiguously magmatic origin.  
 481 Thompson gives its composition as approximately Fe<sub>0.26</sub> Mg<sub>0.22</sub> Ca<sub>0.52</sub> CO<sub>3</sub>. We find it interesting



482 that the Swartbooisdrif ferrocarbonatite has a composition nearly identical to that of Ankerite,  
483  $\text{Ca}(\text{Mg,Fe})(\text{CO}_3)_2$ . If  $\text{FeCO}_3$  behaves similarly to  $\text{MgCO}_3$ , we might expect an equilibrium liquid  
484 composition resulting from partial melting that is roughly equal parts Fe and Mg to be energetically  
485 favorable within the  $\text{FeCO}_3$ - $\text{MgCO}_3$ - $\text{CaCO}_3$  ternary. Given the lack of natural samples, the  
486 energetic and volumetric properties predicted by our simulations, and the measured Fe-contents  
487 found in melting experiments on carbonated mantle materials, we find that ferrocarbonatites are  
488 unlikely to have sufficient Fe-enrichment to stagnate in the mantle owing to their large relative  
489 buoyancy.

## 490 5. Conclusions

491 We perform classical MD simulations of  $\text{MgCO}_3$ -bearing liquids using the empirical  
492 potential model of Hurt and Wolf (2018) at mantle pressures and temperatures. We find that  
493  $\text{MgCO}_3$  liquid assumes a novel topology characterized by four-fold coordination of  $\text{Mg}^{2+}$  with  
494 both the carbonate molecule and  $\text{O}^{2-}$ . Such a structure is markedly different from that of the other  
495 alkaline earth carbonate liquids in which the metal cation is in 6-fold coordination with the  
496 carbonate molecule and 7-8 fold coordination with oxygen atoms. The liquid structure and  
497 resulting thermodynamic properties of  $\text{MgCO}_3$  are found to be more similar to that of  $\text{Li}_2\text{CO}_3$  than  
498 other alkaline earth carbonate liquids, resulting in a dramatically more buoyant and compressible  
499 liquid than previous studies have suggested. The voluminous structure and subsequent low density  
500 of  $\text{MgCO}_3$ -rich liquids bolsters the density contrast of  $\text{MgCO}_3$ -bearing carbonatite melts in the  
501 mantle, increasing their already significant rates of ascent and preventing even relatively dense  
502 ferrocarbonatite melts from achieving a density crossover with the surrounding mantle.

503 The simulations have further suggested that  $\text{MgCO}_3$  molar volume, thermal expansivity,  
504 compressibility, enthalpy and heat capacity do not mix ideally with  $(\text{Ca, Sr, Ba})\text{CO}_3$  liquids. Non-  
505 ideal mixing of volumetric properties stems from localized metal cation ordering around the  $\text{Mg}^{2+}$   
506 ion. We find that it is energetically favorable to surround tetrahedral  $\text{Mg-CO}_3$  complexes with  
507 octahedral Ca-, Sr-, Ba-carbonate complexes. This effect gradually diminishes with pressure,  
508 where  $\text{MgCO}_3$  molar volume is found to mix near-ideally with  $\text{CaCO}_3$ - $\text{SrCO}_3$ - $\text{BaCO}_3$  liquids by  
509 12 GPa. On the other hand, non-ideal mixing of enthalpy in  $\text{MgCO}_3$ -bearing systems persists even  
510 at high pressure.

511 The novel topology of  $\text{MgCO}_3$  liquid indicated by our simulations opens questions on  
512 another important component in mantle-derived carbonatite melts:  $\text{FeCO}_3$ . Given the similar ionic

513 radii of  $\text{Fe}^{2+}$  and  $\text{Mg}^{2+}$ , it's possible that  $\text{Fe}^{2+}$  also assumes a 4-fold coordination with  $(\text{CO}_3)^{2-}$  and  
514  $\text{O}^{2-}$  in  $\text{FeCO}_3$  liquid, producing a similar liquid structure to  $\text{MgCO}_3$ ; the result would be a  $\text{FeCO}_3$   
515 component that is significantly less dense than what has been expected by other studies (e.g. Kang  
516 and Schmidt 2016, 2017). Such a voluminous  $\text{FeCO}_3$  component would inhibit ferrocarnatite  
517 melts generated within subducting slabs from ever stagnating or sinking in the mantle, due to their  
518 low relative densities. Multi-angle energy dispersive X-ray diffraction experiments on  $\text{MgCO}_3$ -  
519 and  $\text{FeCO}_3$ -bearing melts are needed in order to verify the liquid structure of these important  
520 carbonate components.

521

522 **Acknowledgements:** The authors would like to acknowledge Becky Lange, Udo Becker, Youxue  
523 Zhang and Will Bender for their helpful comments throughout the development of the research.  
524 S.H and A.S.W. thank NSF-1763189 for primary financial support for this work, and S.H. also  
525 thanks the Rackham Merit Fellowship for additional financial support.

526

527

## References

- 528  
529 Berendsen H. J. C., Postma J. P. M., van Gunsteren W. F., DiNola a and Haak J. R. (1984)  
530 Molecular dynamics with coupling to an external bath. *J. Chem. Phys.* **81**, 3684–3690.
- 531 Berman R. G. and Brown T. H. (1985) Heat capacity of minerals in the system Na<sub>2</sub>O-K<sub>2</sub>O-CaO-  
532 MgO-FeO-Fe<sub>2</sub>O<sub>3</sub>-Al<sub>2</sub>O<sub>3</sub>-SiO<sub>2</sub>-TiO<sub>2</sub>-H<sub>2</sub>O-CO<sub>2</sub>: representation, estimation, and high  
533 temperature extrapolation. *Contrib. to Mineral. Petrol.* **89**, 168–183.
- 534 Biellmann C., Gillet P., Guyot F., Peyronneau J. and Reynard B. (1993) Experimental evidence  
535 for carbonate stability in the Earth's lower mantle. *Earth Planet. Sci. Lett.* **118**, 31–41.
- 536 Blundy J. and Dalton J. (2000) Experimental comparison of trace element partitioning between  
537 clinopyroxene and melt in carbonate and silicate systems, and implications for mantle  
538 metasomatism. *Contrib. to Mineral. Petrol.* **139**, 356–371.
- 539 Cormier L. and Cuello G. J. (2013) Structural investigation of glasses along the MgSiO<sub>3</sub>-CaSiO<sub>3</sub>  
540 join: Diffraction studies. *Geochim. Cosmochim. Acta* **122**, 498–510.
- 541 Dalton J. A. and Presnall D. C. (1998) Carbonatitic melts along the solidus of model lherzolite in  
542 the system CaO-MgO-Al<sub>2</sub>O<sub>3</sub>-SiO<sub>2</sub>-CO<sub>2</sub> from 3 to 7 GPa. *Contrib. to Mineral. Petrol.* **131**,  
543 123–135.
- 544 Dalton J. A. and Wood B. J. (1993) The compositions of primary carbonate melts and their  
545 evolution through wallrock reaction in the mantle. *Earth Planet. Sci. Lett.* **119**, 511–525.
- 546 Dasgupta R. and Hirschmann M. M. (2006) Melting in the Earth's deep upper mantle caused by  
547 carbon dioxide. *Nature* **440**, 659–662.
- 548 Dasgupta R. and Hirschmann M. M. (2007) Effect of variable carbonate concentration on the  
549 solidus of mantle peridotite. *Am. Mineral.* **92**, 370–379.
- 550 Dasgupta R. and Hirschmann M. M. (2010) The deep carbon cycle and melting in Earth's interior.  
551 *Earth Planet. Sci. Lett.* **298**, 1–13.

- 552 Datta R. K., Roy D. M., Faile S. P. and Tuttle O.F. (1964) Glass formation in carbonate systems.  
553 *J. Am. Ceram. Soc.* **47**, 153. <https://doi.org/10.1111/j.1151-2916.1964.tb14377.x>
- 554 Feinsein H. I. (1984) Diagonal relationships—Descriptive or theoretical? *J. Chem. Educ.* **61**, 128.
- 555 Genge M. J., Price G. D. and Jones A.P. (1995) Molecular dynamics simulations of CaCO<sub>3</sub> melts  
556 to mantle pressures and temperatures: implications for carbonatite magmas *Earth Planet. Sci.*  
557 *Lett.* **131**, 225-238.
- 558 Ghiorso M. S., Hirschmann M. M., Reiners P. W. and Kress V. C. (2002) The pMELTS: A revision  
559 of MELTS for improved calculation of phase relations and major element partitioning related  
560 to partial melting of the mantle to 3 GPa. *Geochemistry Geophys. Geosystems* **3**, 36.
- 561 Ghosh S., Ohtani E., Litasov K. D. and Terasaki H. (2009) Solidus of carbonated peridotite from  
562 10 to 20 GPa and origin of magnesiocarbonatite melt in the Earth's deep mantle. *Chem. Geol.*  
563 **262**, 17–28.
- 564 Green D. H., Wallace M. E. (1988) Mantle metasomatism by ephemeral carbonatite melts. *Nature*  
565 **336**, 459–462.
- 566 Hammouda T. (2003) High-pressure melting of carbonated eclogite and experimental constraints  
567 on carbon recycling and storage in the mantle. *Earth Planet. Sci. Lett.* **214**, 357–368.
- 568 Hoover W. G. (1985) Canonical dynamics: Equilibrium phase-space distributions. *Phys. Rev. A*  
569 **31**, 1695–1697.
- 570 Hurst H. J. (1991) The thermal decomposition of magnesite in nitrogen. *Thermochim. Acta* **189**,  
571 91–96.
- 572 Hurt S.M. (2018) The thermodynamic properties and structure of alkali and alkaline earth  
573 carbonate melts, Ph.D. thesis, University of Michigan, Ann Arbor.

- 574 Hurt S. M. and Lange R. A. (2019) The density of  $\text{Li}_2\text{CO}_3\text{-Na}_2\text{CO}_3\text{-K}_2\text{CO}_3\text{-Rb}_2\text{CO}_3\text{-Cs}_2\text{CO}_3\text{-}$   
575  $\text{CaCO}_3\text{-SrCO}_3\text{-BaCO}_3$  liquids: New measurements, ideal mixing, and systematic trends with  
576 cation coordination. *Geochim. Cosmochim. Acta* **248**, 123–137.
- 577 Hurt S. M. and Wolf A. S. (2018) Thermodynamic properties of  $\text{CaCO}_3\text{-SrCO}_3\text{-BaCO}_3$  liquids: a  
578 molecular dynamics study using new empirical atomic potentials for alkaline earth  
579 carbonates. *Phys. Chem. Miner.* [https://doi-org.proxy.lib.umich.edu/10.1007/s00269-018-](https://doi-org.proxy.lib.umich.edu/10.1007/s00269-018-0995-5)  
580 [0995-5](https://doi-org.proxy.lib.umich.edu/10.1007/s00269-018-0995-5)
- 581 Irving A. J. and Wyllie P. J. (1975) Subsolidus and melting relationships for calcite, magnesite  
582 and the join  $\text{CaCO}_3\text{-MgCO}_3$  36 kb. *Geochim. Cosmochim. Acta* **39**, 35–53.
- 583 Kang N. and Schmidt M. W. (2017) The melting of subducted banded iron formations. *Earth*  
584 *Planet. Sci. Lett.* **476**, 165–178.
- 585 Kang N., Schmidt M. W., Poli S., Connolly J. A. D. and Franzolin E. (2016) Melting relations in  
586 the system  $\text{FeCO}_3\text{-MgCO}_3$  and thermodynamic modelling of Fe-Mg carbonate melts.  
587 *Contrib. to Mineral. Petrol.* **171**, 1-16.
- 588 Katsura T. and Ito E. (1990) Melting and subsolidus phase relations in the  $\text{MgSiO}_3\text{-MgCO}_3$  system  
589 at high pressures: implications to evolution of the Earth's atmosphere. *Earth Planet. Sci. Lett.*  
590 **99**, 110–117.
- 591 Kono Y., Kenney-Benson C., Hummer D., Ohfuji H., Park C., Shen G., Wang Y., Kavner A. and  
592 Manning C. E. (2014) Ultralow viscosity of carbonate melts at high pressures. *Nat. Commun.*  
593 **5**, 5091.
- 594 Kohara S. (1999) A reverse Monte Carlo study of molten lithium carbonate. *Plasmas & Ions* **83**,  
595 79–83.
- 596 Kress V. C., Williams Q. and Carmichael I. S. E. (1988) Ultrasonic investigation of melts in the  
597 system  $\text{Na}_2\text{O-Al}_2\text{O}_3\text{-SiO}_2$ . *Geochim. Cosmochim. Acta* **52**, 283–293.

598 Kroeker S. and Stebbins J. F. (2000) Magnesium coordination environments in glasses and  
599 minerals: New insight from high-field magnesium-25 MAS NMR. *Am. Mineral.* **85**, 1459–  
600 1464.

601 Kubicki J. D., Hemley R. J. and Hofmeister A. M. (1992) Raman and infrared study of pressure-  
602 induced structural changes in MgSiO<sub>3</sub>, CaMgSi<sub>2</sub>O<sub>6</sub>, and CaSiO<sub>3</sub> glass. *Am. Mineral.* **77**, 258-  
603 262.

604 Lange R. A. (1997) A revised model for the density and thermal expansivity of K<sub>2</sub>O-Na<sub>2</sub>O-CaO-  
605 MgO-Al<sub>2</sub>O<sub>3</sub>-SiO<sub>2</sub> liquids from 700 to 1900 K: extension to crustal magmatic temperatures.  
606 *Contrib. to Mineral. Petrol.* **130**, 1–11.

607 Lange R. A. and Carmichael I. S. E. (1987) Densities of Na<sub>2</sub>O-K<sub>2</sub>O-CaO-MgO-FeO-Fe<sub>2</sub>O<sub>3</sub>-Al<sub>2</sub>O<sub>3</sub>-  
608 TiO<sub>2</sub>-SiO<sub>2</sub> liquids: New measurements and derived partial molar properties. *Geochim.*  
609 *Cosmochim. Acta* **51**, 2931–2946.

610 Liu Q. and Lange R. A. (2003) New density measurements on carbonate liquids and the partial  
611 molar volume of the CaCO<sub>3</sub> component. *Contrib. to Mineral. Petrol.* **146**, 370–381.

612 Morizet Y., Paris M., Sifré D., Di Carlo I. and Gaillard F. (2017) The effect of Mg concentration  
613 in silicate glasses on CO<sub>2</sub> solubility and solution mechanism: Implication for natural  
614 magmatic systems. *Geochim. Cosmochim. Acta* **198**, 115–130.

615 Nosé S. (1984) A unified formulation of the constant temperature molecular dynamics methods.  
616 *J. Chem. Phys.* **81**, 511.

617 O’Leary M. C., Lange R. A. and Ai Y. (2015) The compressibility of CaCO<sub>3</sub>-Li<sub>2</sub>CO<sub>3</sub>-Na<sub>2</sub>CO<sub>3</sub>-  
618 K<sub>2</sub>CO<sub>3</sub> liquids: Application to natrocarbonatite and CO<sub>2</sub>-bearing nephelinite liquids from  
619 Oldoinyo Lengai. *Contrib. to Mineral. Petrol.* **170**, 1-18.

620 Plimpton S. (1995) Fast parallel algorithm for short-range molecular dynamics. *J. Comput.*  
621 *Phys.* **117**, 1-42.

- 622 Powell R. and Holland T. J. B. (1988) An internally consistent dataset with uncertainties and  
623 correlations: 3. Applications to geobarometry, worked examples and a computer program. *J.*  
624 *Metamorph. Geol.* **62**, 173–204.
- 625 Ragone S. E., Datta R. K., Roy D. M. and Tuttle O. F. (1966) The System Potassium Carbonate—  
626 Magnesium Carbonate. *J. Phys. Chem.* **70**, 3360-3361. DOI: 10.1021/j100882a515
- 627 Roest D. L., Ballone P., Bedeaux D. and Kjelstrup S. (2017) Molecular dynamics simulations of  
628 metal/molten alkali carbonate interfaces. *J. Chem. Phys. C.* **121**, 17827-17847.
- 629 Roy R. (1950) Magnesium in fourfold coordination in glass. *J. Am. Chem. Soc.* **72**, 3307-3308
- 630 Sharma, S. K. and Simons B. (1980) Raman study of K<sub>2</sub>CO<sub>3</sub>-MgCO<sub>3</sub> glasses. Carnegie Institute.  
631 **79**, 322-326.
- 632 Shimoda K., Nemoto T. and Saito K. (2008) Local structure of magnesium in silicate glasses: a  
633 <sup>25</sup>Mg 3QMAS NMR study. *J. Phys. Chem. B* **112**, 6747–6752.
- 634 Staudigel H., Hart S. R., Schmincke H. U. and Smith B. M. (1989) Cretaceous ocean crust at DSDP  
635 Sites 417 and 418: Carbon uptake from weathering versus loss by magmatic outgassing.  
636 *Geochim. Cosmochim. Acta* **53**, 3091–3094.
- 637 Thompson R., Smith P., Gibson S., Matthey D. and Dickin A. (2002) Ankerite carbonatite from  
638 Swartbooisdrif, Namibia: the first evidence for magmatic ferrocarnatite. *Contrib. to*  
639 *Mineral. Petrol.* **143**, 377–396.
- 640 Trcera N., Cabaret D., Rossano S., Farges F., Flank A. M. and Lagarde P. (2009) Experimental  
641 and theoretical study of the structural environment of magnesium in minerals and silicate  
642 glasses using X-ray absorption near-edge structure. *Phys. Chem. Miner.* **36**, 241–257.
- 643 Vinograd V. L., Winkler B., Putnis A., Gale J. D. and Sluiter M. H. F. (2006) Static lattice energy  
644 calculations of mixing and ordering enthalpy in binary carbonate solid solutions. *Chem. Geol.*  
645 **225**, 304–313.

- 646 Vuilleumier R., Seitsonen A., Sator N. and Guillot B. (2014) Structure, equation of state and  
647 transport properties of molten calcium carbonate (CaCO<sub>3</sub>) by atomistic simulations. *Geochim.*  
648 *Cosmochim. Acta* **141**, 547–566.
- 649 Waseda, Y. and Toguri, J.M. (1977) The structure of molten binary silicate systems CaO-SiO<sub>2</sub> and  
650 MgO-SiO<sub>2</sub> *Metall. Mater. Trans. B* **8**, 563–568. <https://doi.org/10.1007/BF02669331>



**Table 1.** The thermodynamic properties of MgCO<sub>3</sub> liquid as derived from the simulations. These are fitted parameters of both a 3<sup>rd</sup> and 4<sup>th</sup> order Birch-Murnaghan EOS (Eqs. A1-A4) that have been fitted to the simulations of MgCO<sub>3</sub> liquid from 773 to 2000 K up to 20 GPa by the least squares method.  $V_{Tr,0}$  is the molar volume at 1100 K and 1 bar;  $\alpha$  is the thermal expansion;  $K_{Tr,0}$  is the bulk modulus at 1 bar and 1100 K and  $\delta K_0/\delta T$  is its temperature dependence;  $K'$  and  $K''$  are first- and second-pressure derivatives of the bulk modulus. The root mean square of the pressure residuals of the 4<sup>th</sup> order fit is 0.02 GPa and of the volume residuals is 0.27 cm<sup>3</sup>/mol.

Property	Best Fit ( $1\sigma$ )	
	3 <sup>rd</sup> order EOS	4 <sup>th</sup> order EOS
RMS Press. residual (GPa)	0.11	<b>0.02</b>
$V_{Tr,0}$ (cm <sup>3</sup> /mol)	46.0(2)	<b>44.21(9)</b>
$\alpha$ ( $10^{-4} \cdot \text{K}^{-1}$ )	0.004(13)	<b>1.07(14)</b>
$K_{Tr,0}$ (GPa)	0.9(20)	<b>6.15(15)</b>
$\delta K_0/\delta T$ ( $10^{-3} \cdot \text{GPa/K}$ )	-0.1(18)	<b>-1.37(35)</b>
$K'$	33(75)	<b>2.41(1)</b>
$K''$		<b>3.16(1)</b>

**Table 2.** Simulated densities of (Ca, Mg)CO<sub>3</sub> binary liquids approximating compositions of carbonatite melts from phase equilibrium experiments of carbonated mantle (Dalton and Wood 1993, Dalton and Presnall 1998, Hammouda 2003, and Ghosh et al. 2009). The pressures and temperatures of the simulations reflect those of the phase equilibrium experiments. Corrected density adjusts the simulated density to account for small concentrations of FeCO<sub>3</sub> and SiO<sub>2</sub> present in the liquid produced in the original phase equilibrium experiments.

MgCO <sub>3</sub> (mol%)	Press. (GPa)	Temp. (K)	Gram formula wt.	Sim.Vol. (cm <sup>3</sup> /mol)	Sim. ρ (g/cm <sup>3</sup> )	Corrected ρ (g/cm <sup>3</sup> )
Dalton and Wood (1993)						
13.6	1.5	1423	98.22	39.19	2.506	2.507
17.4	1.5	1423	97.69	39.23	2.490	2.497
22.5	2.2	1523	96.95	38.28	2.532	2.545
28.7	2.5	1523	96.05	37.76	2.544	2.558
31.6	2.8	1573	95.63	37.47	2.552	2.573
35.1	3.0	1573	95.11	37.09	2.564	2.585
Dalton and Presnall (1998)						
40.9	3.0	1518	93.64	36.59	2.559	2.561
44.0	3.5	1543	93.15	35.94	2.592	2.592
45.8	4.0	1563	92.86	35.44	2.620	2.618
49.2	5.0	1603	92.33	34.54	2.673	2.669
50.9	6.0	1653	92.05	33.77	2.726	2.717
55.5	7.0	1703	91.33	33.03	2.765	2.756
Hammouda (2003)						
10.5	6.0	1523	98.43	34.91	2.820	2.871
10.9	7.0	1273	98.36	33.61	2.927	2.957
10.8	10.0	1373	98.38	32.23	3.052	3.086
14.1	10.0	1473	97.86	32.47	3.014	3.068
Ghosh et al (2009)						
87.1	12.5	1873	86.35	29.53	2.925	3.071
86.8	13.5	1823	86.40	29.12	2.967	3.096
61.1	15.0	1873	90.45	29.62	3.053	3.133
76.1	17.5	1833	88.08	28.30	3.112	3.182

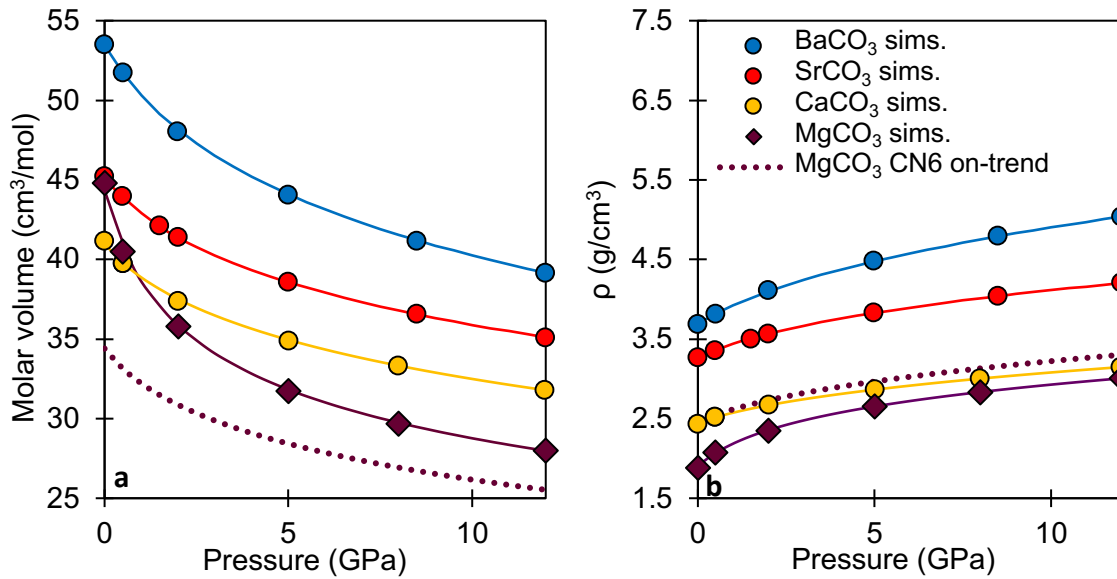


**Figure 1.** Compression curve of MgCO<sub>3</sub> liquid strongly deviates from expectations based on the other alkaline-earth carbonates. Panel a shows simulated molar volumes at 1100 K as a function of pressure for MgCO<sub>3</sub>, CaCO<sub>3</sub>, SrCO<sub>3</sub> and BaCO<sub>3</sub> liquids. Points show simulation results, while solid lines represent best-fit Birch-Murnaghan EOS for each liquid (3<sup>rd</sup> order for CaCO<sub>3</sub>, SrCO<sub>3</sub> and BaCO<sub>3</sub> and 4<sup>th</sup> order for MgCO<sub>3</sub>). The dotted line represents the expected compression curve of MgCO<sub>3</sub> if its volumetric properties were in-line with periodic trends observed among the other alkaline earth carbonates (i.e. if Mg-C coordination was 6-fold rather than 4). As evident, CaCO<sub>3</sub>, SrCO<sub>3</sub> and BaCO<sub>3</sub> form nearly parallel curves that increase systematically from Ca to Ba, while MgCO<sub>3</sub> liquid deviates dramatically, especially at low pressure. Panel b shows the same compression curves in terms of density.

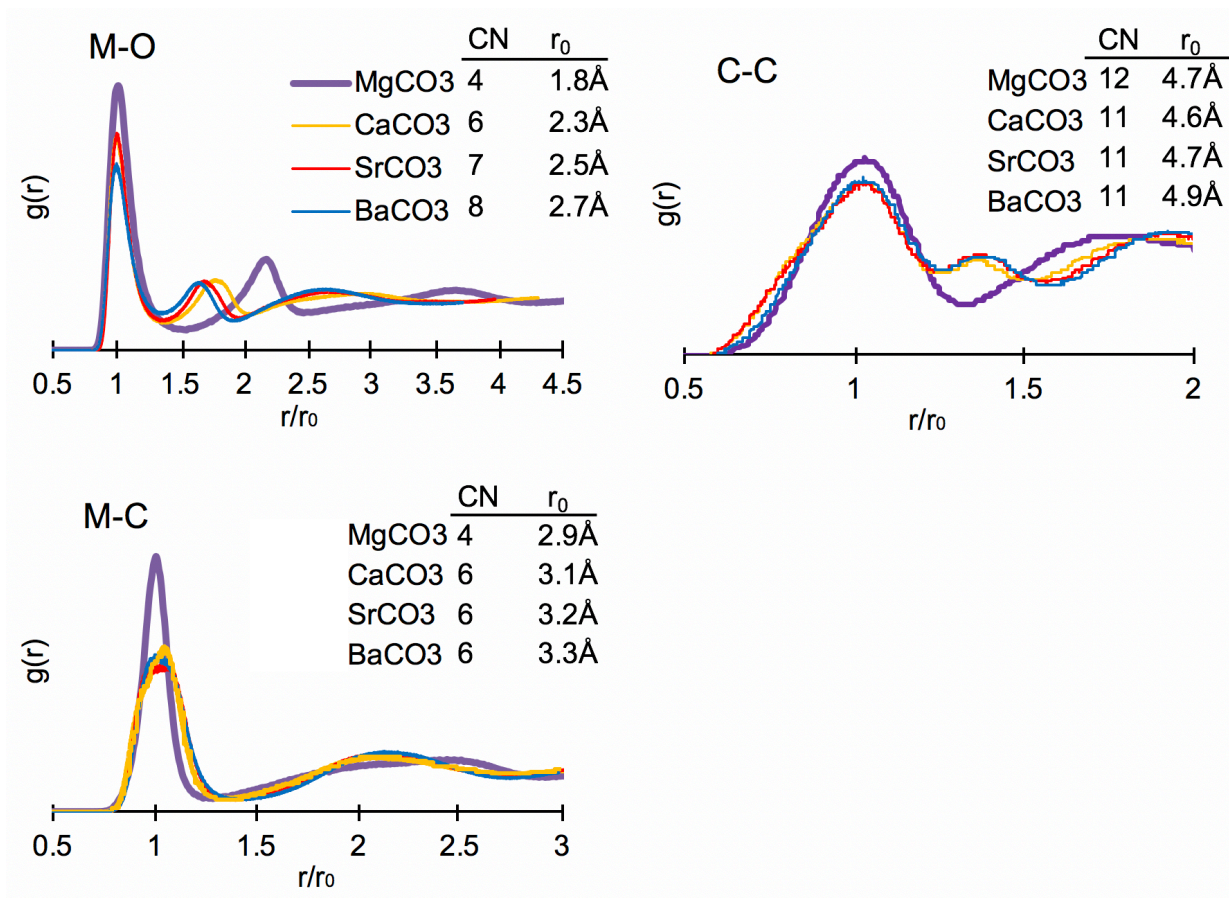


**Figure 2.** Liquid structure of MgCO<sub>3</sub> is distinct from CaCO<sub>3</sub>, SrCO<sub>3</sub> and BaCO<sub>3</sub>. Pair distribution functions are calculated from liquid simulations at 1 bar and 1100 K for atomic pairs between carbon (C), oxygen (O) and metal cations (M: Mg, Ca, Sr, Ba). The M-O, C-C and M-C pairs shown in panels a, b and c, respectively. For visual comparison, interatomic separation distance ( $r$ ) has been normalized to the position of the first peak ( $r_0$ ). Average coordination number (CN) has been calculated for each pair in the embedded tables.

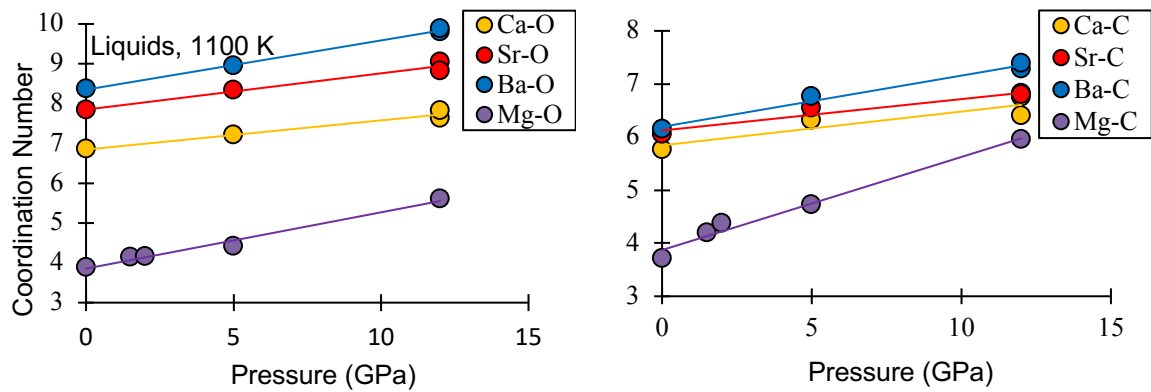


**Figure 3.** The structure of  $\text{MgCO}_3$  liquid becomes progressively more like  $(\text{Ca}, \text{Sr}, \text{Ba})\text{CO}_3$  liquids at high pressure. The simulated evolution of coordination for M-O and M-C pairs (in panels a and b), is shown for pure  $\text{MgCO}_3$ ,  $\text{CaCO}_3$ ,  $\text{SrCO}_3$  and  $\text{BaCO}_3$  liquids as a function of pressure up to 12 GPa. In  $\text{MgCO}_3$ , the coordination of M-O and M-C pairs starts at 4 at 1 bar and approaches  $\sim 6$  at 12 GPa (while other alkaline earths' coordination evolution is more modest, rising 2-4 times slower).

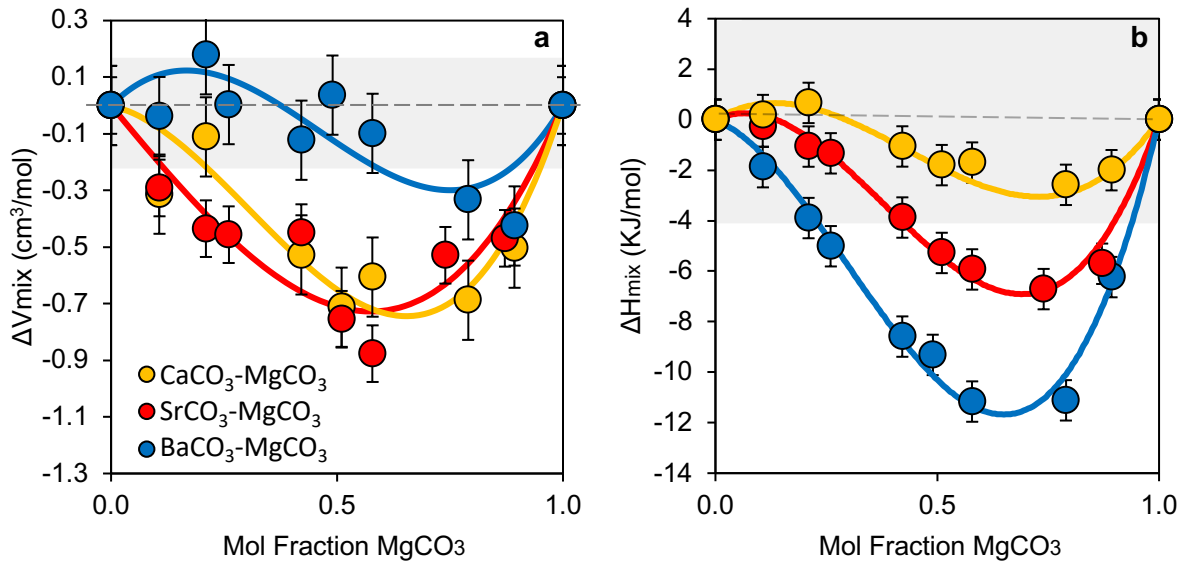


**Figure 4.** Non-ideal mixing dominates volumetric and enthalpic properties in MgCO<sub>3</sub>-bearing systems at 1 bar. The  $\Delta V_{mix}$  (a) and  $\Delta H_{mix}$  (b) of MgCO<sub>3</sub>-bearing binary liquids at 1100 K and 1 bar are shown, with non-zero values indicating non-ideal mixing. The shaded regions reflect the range of  $\Delta V_{mix}$  and  $\Delta H_{mix}$  for the ideal mixing of (Ca, Sr, Ba)CO<sub>3</sub> liquids calculated by Hurt and Wolf (2018). Both  $\Delta V_{mix}$  and  $\Delta H_{mix}$  are, for the most part, negative and reach a minimum at MgCO<sub>3</sub> molar concentrations of 0.6 to 0.8. Points show simulation results and lines are the best-fit sub-regular solutions (Eq. 3).

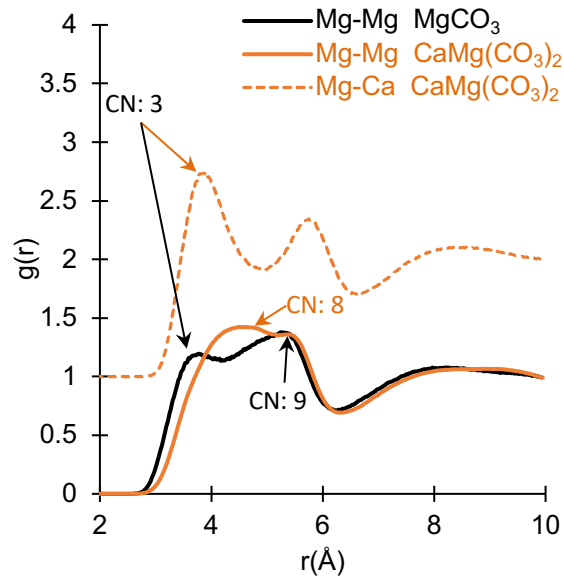


**Figure 5.** Mg-Mg pdf curve in pure  $\text{MgCO}_3$  liquid are significantly altered upon mixing due to  $\text{Mg}^{2+}$  vacating the inner coordination shell in favor of  $\text{Ca}^{2+}$ ,  $\text{Sr}^{2+}$  or  $\text{Ba}^{2+}$  ions. The pdf curves are generated from simulations of pure  $\text{MgCO}_3$  liquid and a mixture,  $\text{CaMg}(\text{CO}_3)_2$ , at 1100 K and 1 bar. The inner coordination shell (CN=3) in pure  $\text{MgCO}_3$  disappears in the mixture and is filled with  $\text{Ca}^{2+}$ . This same effect occurs in  $\text{MgCO}_3$  mixtures with the other alkaline earth cations ( $\text{Sr}^{2+}$  and  $\text{Ba}^{2+}$ ). This likely results from an energetic penalty for  $\text{Mg}^{2+}$  to be surrounded by other  $\text{Mg}^{2+}$  ions; the preferential ordering observed here results from surrounding the  $\text{Mg}-\text{CO}_3$  tetrahedral complexes with the  $(\text{Ca}, \text{Sr}, \text{Ba})^{2+}$  octahedral complexes, and might be favored as a mechanism to handle cation size mismatch that relaxes stresses in the atomic structure.

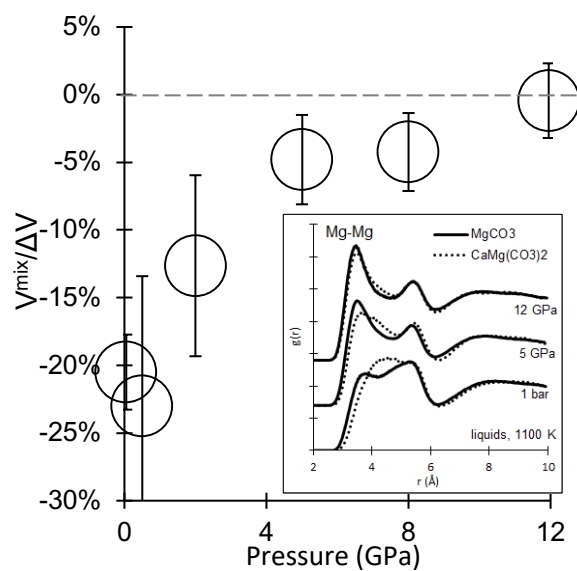


**Figure 6.** Mixing of molar volumes for  $\text{CaCO}_3$  and  $\text{MgCO}_3$  liquid approach ideality with increasing pressure due to a progressively diminishing cation ordering effect.  $V_{mix}$  is shown as a function of pressure normalized to  $\Delta V_{Ca-Mg}$  (which is the difference between pure  $\text{CaCO}_3$  and  $\text{MgCO}_3$  liquid at the given pressure). As pressure increase, the magnitude of non-ideality approaches 0. The figure inset shows corresponding liquid Mg-Mg pdf curves of pure  $\text{MgCO}_3$  (solid lines) and  $\text{CaMg}(\text{CO}_3)_2$  (dotted lines) at 1 bar, 2 and 12 GPa. The disparity between the two curves reflects the degree of cation ordering in the liquid. As pressure increase, the mixed  $\text{CaMg}(\text{CO}_3)_2$  curve conforms to that of pure  $\text{MgCO}_3$ .



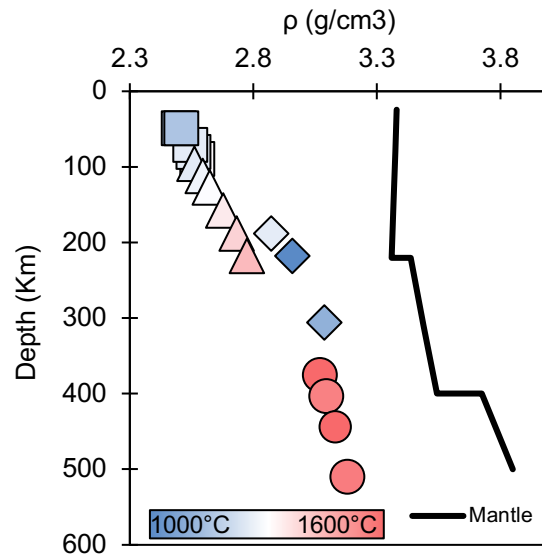


**Figure 7.** The densities of primary carbonatite melts maintain a high negative density contrast with the surrounding mantle. The simulated densities of  $\text{MgCO}_3\text{-CaCO}_3$  binary liquids representing primary carbonatite melts are corrected for minor  $\text{FeCO}_3$  and  $\text{SiO}_2$  concentration and are shown as a function of depth. The simulation temperatures, pressures and compositions are based on the phase equilibrium experiments of Dalton and Wood (1993) (squares), Dalton and Presnall (1998) (triangles), Hammouda (2003) (diamonds) and Ghosh et al. (2009) (circles). Coloring reflects simulation temperature. Mantle density as a function of depth is taken from PREM (Dziewonski and Anderson, 1981).

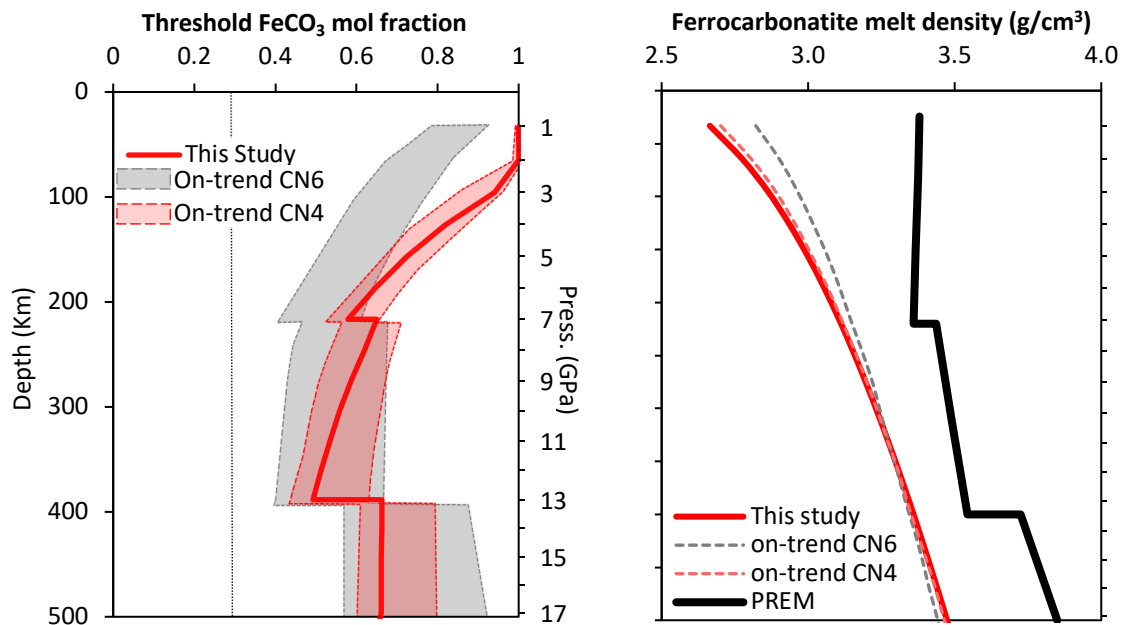


**Figure 8.** Panel a shows the threshold mole percent  $\text{FeCO}_3$  necessary for a hypothetical ferrocarbonatite (with composition  $(\text{Fe}_x, \text{Mg}_{0.5 \cdot (1-x)}, \text{Ca}_{0.5 \cdot (1-x)})\text{CO}_3$ ) to achieve neutral buoyancy in the mantle as a function of depth. Three different estimates are depicted: the red line shows results from this study while the gray- and red-shaded regions represent estimated volumetric properties from Hurt (2018), which assume that both  $\text{Mg}^{2+}$  and  $\text{Fe}^{2+}$  are in 6-fold and 4-fold coordination with carbonate respectively. The dotted vertical dotted line shows the iron concentration of the only natural, unambiguously-magmatic ferrocarbonatite found in the literature (Thompson et al. 2002). Panel b shows the estimated densities of this natural ferrocarbonatite composition ( $\text{Fe}_{0.26} \text{Mg}_{0.22} \text{Ca}_{0.52} \text{CO}_3$ ) calculated for the three models (red lines are simulations from this study and the optimal on-trend CN6 and CN4 models from Hurt 2018 are shown in gray- and red-dashed lines) along with the density of PREM (Dziewonski and Anderson, 1981).

# Appendices

## A. Equations of state used to model simulation data

The simulated molar volumes of  $\text{MgCO}_3$  liquid were used to fit the parameters of the EOS below (adapted from Angel 2000):

$$P = 3K_{T,0}f_E(1 + 2f_E)^{\frac{5}{2}}\{1 + c3 f_E + c4 f_E^2\} \quad \text{Eq. A. 1}$$

$$c3 = \frac{3}{2}(K' - 4), \quad c4 = \frac{3}{2}\left[K_{T,0}K'' + (K' - 4)(K' - 3) + \frac{35}{9}\right]$$

where  $K_{T,0}$  is the isothermal bulk modulus at 1 bar and simulation temperature ( $T$ ),  $c3$  and  $c4$  are the 3<sup>rd</sup> and 4<sup>th</sup> order EOS terms, which are written in terms of the fitted parameters  $K'$  and  $K''$  (the 1<sup>st</sup> and 2<sup>nd</sup> pressure-derivatives of the bulk modulus).  $K_{T,0}$  is a function of temperature according to:

$$K_{T,0}(T) = K_{Tr,0} + \frac{\delta K_0}{\delta T}(T - 1100 \text{ K}) \quad \text{Eq. A. 2}$$

$\left(\frac{\delta K_0}{\delta T}\right)$  is the fitted 1 bar temperature dependence of the bulk modulus and  $K_{T,0}$  is the fitted 1 bar bulk modulus at the reference temperature. The Eulerian finite strain,  $f_E$ , is defined as:

$$f_E = \left[ \left( \frac{V_{T,0}}{V_{T,P}} \right)^{2/3} - 1 \right] / 2 \quad \text{Eq. A. 3}$$

$V_{T,P}$  is the simulation volume at  $T$  and pressure ( $P$ ).  $V_{T,0}$  is the volume at 1 bar and  $T$  and can be calculated from the fitted 1 bar volume at 1100 K ( $V_{Tr,0}$ ) and the fitted thermal expansion ( $\alpha$ ).  $V_{T,0}$  thus becomes:

$$V_{T,0} = V_{Tr,0} e^{\alpha(T-1100 \text{ K})} \quad \text{Eq. A. 4}$$

The parameter  $\alpha$  is the fitted 1 bar thermal expansion coefficient, assumed to be temperature-independent.

## B. Comparison of $\text{MgCO}_3$ to alkali carbonate liquids

MD simulations of  $\text{MgCO}_3$  liquid indicate that, at ambient pressure (where  $\text{MgCO}_3$  liquid is unstable)  $\text{Mg}^{2+}$  assumes a 4-fold coordination with both the carbonate molecule and oxygen much like alkali carbonate liquids,  $\text{Li}_2\text{CO}_3$ ,  $\text{NaCO}_3$  and  $\text{K}_2\text{CO}_3$  (e.g. Roest et al. 2017; Kohara et al. 1999). This stands in stark contrast to  $\text{CaCO}_3$ - $\text{SrCO}_3$ - $\text{BaCO}_3$  liquids in which metal cations are in 6-fold coordination with carbonate and 7- to 8-fold coordination with oxygen (Hurt and Wolf 2018). The similarity between  $\text{MgCO}_3$  and alkali carbonate liquid structure is well-illustrated by a comparison of pdf curves for  $\text{MgCO}_3$  liquid

25 versus  $\text{Li}_2\text{CO}_3$  liquid, as shown in Figure B.1 (Roest et al. 2017). This resemblance in liquid structure (and  
26 physical properties) is not unprecedented; it's partially explained by the Mg-Li diagonal relationship, in  
27 which the compounds of certain elemental pairs (Li-Mg, Be-Al, B-Si and C-P) that are diagonally adjacent  
28 on the Periodic Table, share some properties in common (e.g., Feinstein 1984). Thus, it's expected that  
29 liquid  $\text{MgCO}_3$  volumetric properties should be similar to that of  $\text{Li}_2\text{CO}_3$ .

30 Alkali carbonates generally have a larger volume than their alkaline earth counterparts, not only  
31 because of the additional metal cation per formula unit but because the partial molar volume of  $(\text{CO}_3)^{2-}$  is  
32 greater,  $\sim 38 \text{ cm}^3/\text{mol}$  versus  $31 \text{ cm}^3/\text{mol}$  (Hurt and Lange 2019). The partial molar volume of  $(\text{CO}_3)^{2-}$  is  
33 greater in alkaline earth carbonate liquids because of changes in network topology, not because the size of  
34 the carbonate molecule actually increases (See Hurt and Lange 2019 for a full discussion).

### 35 ***C. Structure and thermodynamics of $\text{MgCO}_3$ -carbonate mixtures***

36 The thermodynamic and structural properties of  $\text{MgCO}_3$ -bearing liquids is explored through molecular  
37 dynamic simulations. The conditions and basic results for each run are summarized in Table C.1, including  
38 simulations of pure  $\text{MgCO}_3$  as well as binary mixtures of  $\text{MgCO}_3$  with  $\text{CaCO}_3$ ,  $\text{SrCO}_3$  and  $\text{BaCO}_3$  liquids.  
39 The detailed results of binary mixtures and associated excess properties are reported in Table C.2, and the  
40 best-fit asymmetric sub-regular solution model parameters are presented in Table C.3.

41 The associated atomic structures of these compositional binary melts are presented in Figures C.1 and  
42 C.2. The liquid structures are shown for all pure endmember melts as well as 50:50 mixtures along each  
43  $\text{MgCO}_3$ -bearing binary in Figure C.1. The complete set of pdfs for each liquid for M-O, M-C, and C-C  
44 pairs are shown for each of these liquids. To better understand the liquid structure with respect to carbon-  
45 carbon pairs, the pdfs of  $\text{MgCO}_3$ ,  $\text{CaCO}_3$ , and  $\text{CaMg}(\text{CO}_3)_2$  liquid are shown in Figure C.2, along with a  
46 theoretical weighted average of the endmembers.

### 47 ***D. Description of density simulation corrections***

48 The simulation results presented in the main text highlight the novel topology of  $\text{MgCO}_3$  liquid and  
49 provide estimates of its thermodynamic properties and mixing behavior which is important for future  
50 integration of the  $\text{MgCO}_3$  liquid component into thermodynamic modeling software such as MELTS or  
51 THERMOCALC. However, the pair potential model can also be directly applied to geologic systems by  
52 providing property estimates of natural carbonatite liquids at relevant temperatures and pressures. In order  
53 to estimate the density of primary carbonatite melts generated by low-degree partial melting of carbonated  
54 mantle, simulations are performed in the  $\text{CaCO}_3$ - $\text{MgCO}_3$  liquid system. The simulated liquid compositions,

55 temperatures and pressures are based on the results of phase equilibrium experiments carbonated mantle  
56 partial melting experiments.

57 To constrain the composition of carbonatite melts produced by partial melting of the carbonated mantle,  
58 Dalton and Wood (1993) and Dalton and Presnall (1998) conducted phase equilibrium experiments on  
59 carbonated peridotite systems at pressures ranging from 1.5 to 7 GPa and temperatures from 1423 to 1703  
60 K. Hammouda (2003) and Ghosh et al. (2009) conducted similar experiments for carbonated eclogite in the  
61 6-17.5 GPa pressure range. They produced carbonate melts with > 92 wt. % CaCO<sub>3</sub> and MgCO<sub>3</sub> for the  
62 peridotite-derived melts and > 88 wt. % for the eclogite-derived. The remaining wt. % is mostly FeCO<sub>3</sub> and  
63 SiO<sub>2</sub>. We estimate the densities of the primary carbonate melts of Dalton and Wood (1993), Dalton and  
64 Presnall (1998), Hammouda (2003) and Ghosh et al. (2009) by simplifying them to CaCO<sub>3</sub>-MgCO<sub>3</sub> binary  
65 compositions and simulating them at their respective temperature and pressure conditions. The simulated  
66 CaCO<sub>3</sub>-MgCO<sub>3</sub> melts range in density between 2.49 to 3.11 g/cm<sup>3</sup> at 1.5 and 17.5 GPa respectively; the full  
67 results are presented in Table 2. Since the minor FeCO<sub>3</sub> and SiO<sub>2</sub> components are omitted in these  
68 simulations, the raw simulated densities have been corrected to account for their absence.

69 An approximate correction to the simulated densities may be made by assuming FeCO<sub>3</sub> has the same  
70 partial molar volume as the MgCO<sub>3</sub> melt component and integrating it into the density calculation. The  
71 density may be further corrected by accounting for the SiO<sub>2</sub> liquid component of the carbonatite melt by  
72 using the volumetric data from Lange and Carmichael (1987) and Kress et al. (1988) and assuming the SiO<sub>2</sub>  
73 volume mixes ideally into the carbonate melt. Table 2 gives the simulated melt composition, gram formula  
74 weight, molar volume and simulated density along with the FeCO<sub>3</sub>-SiO<sub>2</sub>-corrected density.

75

76 **Table C.1.** The complete simulation results are shown below. Total energy and Enthalpy are relative to  
 77 their respective values for  $\text{MgCO}_3$  at 1100 K and 0 GPa. 1  $\sigma$  error on temperature is 2 K, 0.02 GPa for  
 78 pressure, 0.1  $\text{cm}^3/\text{mol}$  for volume, 0.2 KJ for total energy and 0.9 KJ for enthalpy.

	Temp. (K)	Press. (GPa)	Mol. Vol. ( $\text{cm}^3/\text{mol}$ )	Tot. Energy (KJ/mol)	Enthalpy (KJ/mol)
<b><i>Pure MgCO<sub>3</sub></i></b>					
	773	0.00	43.10	-49	-49
	1100	0.00	44.48	0	0
	1499	0.00	46.46	61	61
	2000	0.00	47.98	136	136
	1099	0.49	40.52	-2	17
	900	1.99	35.39	-32	-
	1101	2.01	35.84	-2	70
	1500	2.02	36.85	58	132
	1869	2.98	35.89	112	219
	2273	3.58	35.97	170	299
	1101	4.99	31.74	2	160
	1101	5.00	31.74	3	161
	1501	5.00	32.66	61	224
	1100	8.00	29.71	8	245
	2274	8.05	31.96	173	430
	1099	12.01	28.03	17	353
	1500	11.99	28.67	72	416
	1099	15.01	27.14	25	432
	2000	14.95	28.41	147	571
	1100	19.99	26.07	39	560
<i>Mol frac. MgCO<sub>3</sub></i>	<b><i>CaCO<sub>3</sub>-MgCO<sub>3</sub> Simulations</i></b>				
0.11	1100	0.00	41.06	196	195
0.12	1424	1.49	39.19	239	298
0.14	1424	1.49	39.28	236	294
0.15	1423	1.54	39.23	232	291
0.15	1372	9.98	32.23	223	544
0.17	1423	1.46	39.14	227	284
0.2	1523	2.21	38.28	235	319
0.21	1099	0.00	43.06	43	43
0.21	1101	0.00	41.62	174	173
0.22	1523	2.20	38.35	230	314
0.22	1523	2.20	38.35	230	314
0.26	1523	2.49	37.76	222	316
0.28	1573	2.83	37.47	224	329
0.29	1525	2.52	37.70	216	310
0.32	1573	2.84	37.33	217	322
0.32	1572	3.03	37.09	216	328
0.35	1518	2.98	36.71	200	309
0.35	1573	3.01	36.99	208	319
0.35	1572	3.01	36.88	208	318
0.4	1544	3.50	36.12	191	317
0.41	1519	2.98	36.59	187	296

0.42	1100	-0.01	41.94	126	125
0.44	1543	3.50	35.94	184	309
0.46	1563	4.00	35.44	183	324
0.51	1100	-0.01	42.06	105	104
0.51	1100	-0.01	42.06	105	104
0.51	1998	0.01	46.60	249	249
0.51	1100	0.50	40.05	104	124
0.51	1100	2.00	36.41	102	174
0.51	1799	2.98	37.15	207	317
0.51	1800	2.99	37.16	207	318
0.51	1573	4.98	34.42	176	347
0.51	1099	4.99	33.13	103	268
0.51	1603	5.02	34.54	181	354
0.51	1655	5.98	33.77	184	386
0.51	1100	8.00	31.33	108	358
0.51	1100	12.00	29.86	117	475
0.56	1703	7.03	33.03	183	414
0.58	1102	0.00	42.41	91	90
0.61	1873	14.97	29.62	205	648
0.76	1834	17.48	28.30	174	668
0.79	1099	0.00	43.06	43	43
0.87	1873	12.48	29.53	150	518
0.87	1821	13.54	29.12	145	538
<b><i>SrCO<sub>3</sub>-MgCO<sub>3</sub> Simulations</i></b>					
0.11	1100	0.01	44.89	291	291
0.21	1100	0.00	44.66	257	256
0.26	1101	-0.01	44.60	240	239
0.42	1099	0.01	44.48	185	185
0.49	1100	11.99	31.51	172	549
0.51	1100	0.00	44.11	154	154
0.51	2000	0.03	48.71	299	300
0.58	1100	-0.01	43.93	131	131
0.74	1100	0.01	44.15	78	78
0.87	1100	0.00	44.11	36	36
<b><i>BaCO<sub>3</sub>-MgCO<sub>3</sub> Simulations</i></b>					
0.11	1100	0.00	52.52	422	421
0.26	1101	0.00	51.18	346	346
0.42	1099	0.01	49.59	266	266
0.49	2000	-0.02	53.57	373	372
0.49	1099	12.00	33.60	247	650
0.58	1100	0.00	48.19	189	188
0.79	1099	0.00	46.04	89	88
0.89	1100	0.01	45.02	45	45

79

80

81 **Table C.2:** The volume and enthalpy results of MgCO<sub>3</sub>-bearing binary simulations at 1100 K and 1 bar are  
 82 shown below. Ideal volumes and enthalpies and  $\Delta V_{mix}$  and  $\Delta H_{mix}$  calculated according to Eq. 7 and 8 are  
 83 also listed.

Comp. Mol%MgCO <sub>3</sub>	Mol. Vol. (cm <sup>3</sup> /mol)	Ideal Vol. (cm <sup>3</sup> /mol)	$\Delta V_{mix}$ (cm <sup>3</sup> /mol)	Enthalpy (KJ/mol)	Ideal H (KJ/mol)	$\Delta H_{mix}$ (KJ/mol)
<b><i>CaCO<sub>3</sub>-MgCO<sub>3</sub></i></b>						
0.0	41.00	41.00	0.00	218.9	218.9	0.0
10.7	41.06	41.37	-0.31	195.7	195.5	0.2
21.0	41.62	41.73	-0.11	173.6	173.0	0.7
42.1	41.94	42.47	-0.53	125.6	126.7	-1.1
51.0	42.06	42.78	-0.71	105.4	107.2	-1.8
57.9	42.41	43.01	-0.61	90.5	92.2	-1.7
79.0	43.06	43.75	-0.69	43.4	46.0	-2.6
89.3	43.60	44.11	-0.50	21.5	23.5	-2.0
100.0	44.48	44.48	0.00	0.0	0.0	0.0
<b><i>SrCO<sub>3</sub>-MgCO<sub>3</sub></i></b>						
0.0	45.26	45.26	0.00	326.0	326.0	0.0
10.7	44.89	45.18	-0.29	290.8	291.1	-0.3
21.0	44.66	45.10	-0.44	256.5	257.6	-1.1
26.0	44.60	45.06	-0.46	239.9	241.2	-1.3
42.1	44.48	44.93	-0.45	184.8	188.7	-3.9
51.0	44.11	44.86	-0.76	154.4	159.7	-5.3
57.9	43.93	44.81	-0.88	131.4	137.3	-5.9
74.0	44.15	44.68	-0.53	78.1	84.8	-6.7
87.2	44.11	44.58	-0.47	36.1	41.8	-5.7
100.0	44.48	44.48	0.00	0.0	0.0	0.0
<b><i>BaCO<sub>3</sub>-MgCO<sub>3</sub></i></b>						
0.0	53.53	53.53	0.00	475.0	475.0	0.0
10.7	52.52	52.56	-0.04	422.2	424.1	-1.9
21.0	51.81	51.63	0.18	371.4	375.3	-3.9
26.0	51.18	51.17	0.00	346.4	351.4	-5.0
42.1	49.59	49.71	-0.12	266.3	274.9	-8.6
49.0	49.13	49.09	0.04	233.0	242.3	-9.3
57.9	48.19	48.29	-0.10	188.9	200.1	-11.2
79.0	46.04	46.38	-0.33	88.6	99.7	-11.1
89.3	45.02	45.45	-0.43	44.7	50.9	-6.2
100.0	44.48	44.48	0.00	0.0	0.0	0.0

84

85



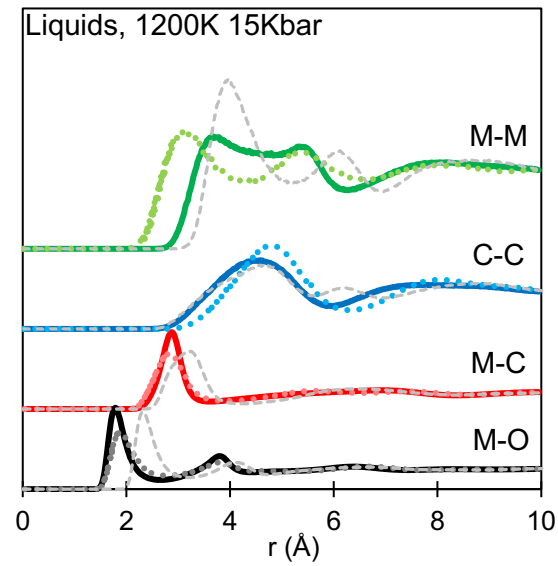
86 **Table C.3:** Gives the coefficients fitted to Eq. 1 to describe both  $\Delta V_{mix}$  and  $\Delta H_{mix}$  calculated by our  
87 simulations of liquids in each of the three binaries at 1100 K and 1 bar.

88

	$\Delta V_{mix}$ (cm <sup>3</sup> /mol)	$\Delta H_{mix}$ (KJ/mol)		
	$w$	$\Delta w$	$w$	$\Delta w$
CaCO <sub>3</sub> -MgCO <sub>3</sub>	-2.91	-6.78	-7.33	-35.51
SrCO <sub>3</sub> -MgCO <sub>3</sub>	-3.625	-3.77	-22.90	-62.56
BaCO <sub>3</sub> -MgCO <sub>3</sub>	-1.345	-6.47	-40.20	-92.95

92

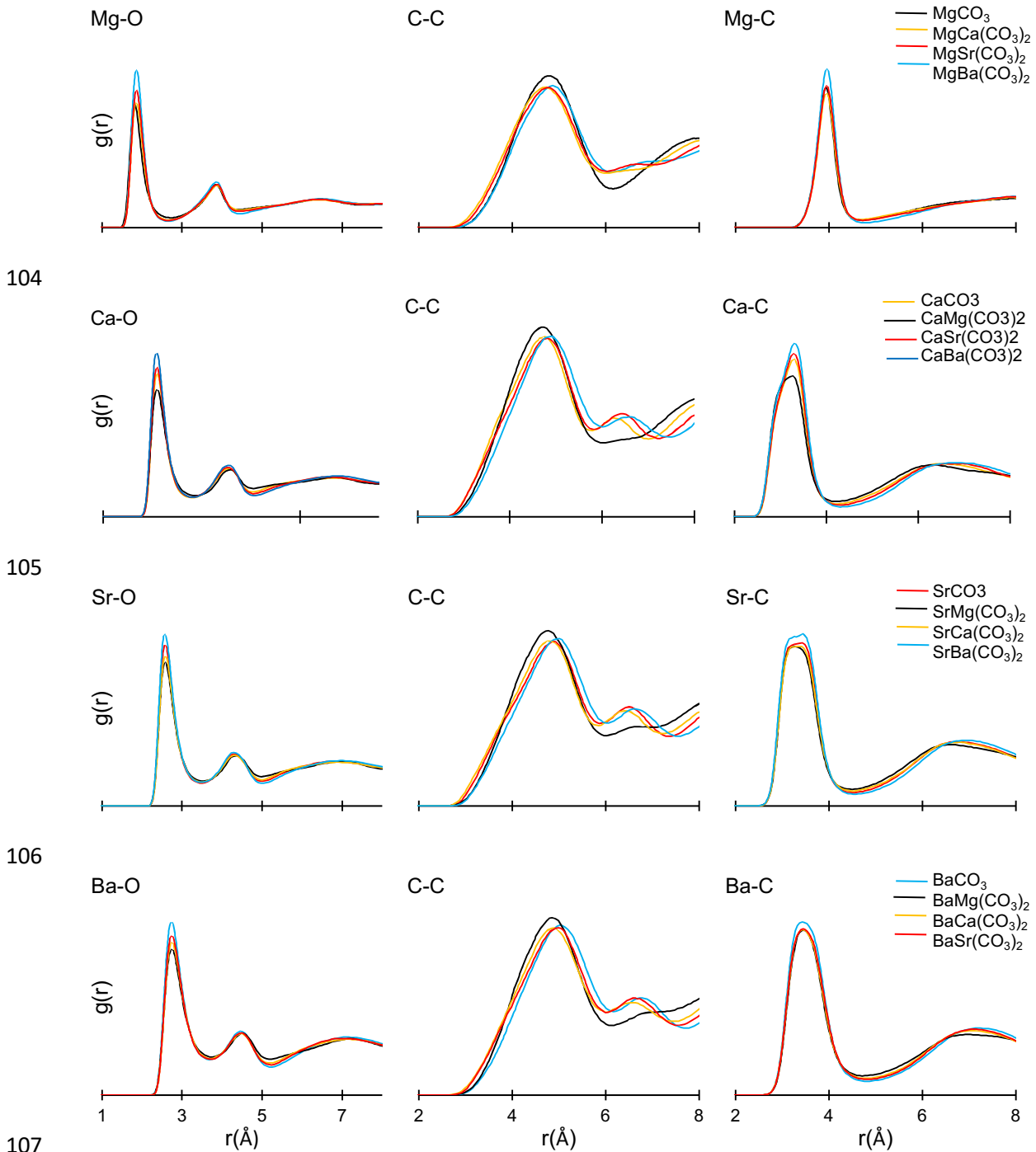
93 **Figure B.1.** The liquid structure of  $\text{MgCO}_3$  is similar to that of  $\text{Li}_2\text{CO}_3$ . The liquid pdf curves of  
94  $\text{MgCO}_3$  from our simulations (solid lines) are compared to those of  $\text{Li}_2\text{CO}_3$  generated by FPMD  
95 simulations from Roest et al. 2017 (dotted lines) at 1200 K and 15 kbar.  $\text{CaCO}_3$  liquid at 1200 K  
96 and 15 kbar is shown for comparison (grey dashed line).  $\text{MgCO}_3$  liquid is more like  $\text{Li}_2\text{CO}_3$  than  
97  $\text{CaCO}_3$ .



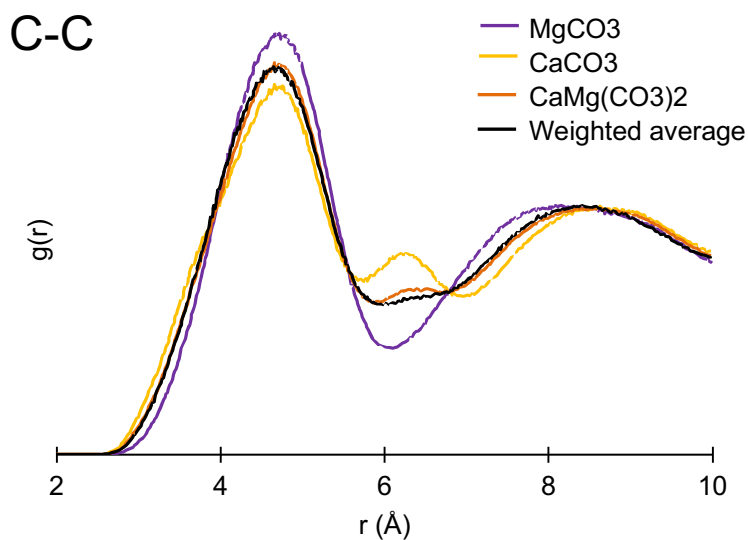
98

99

100 **Figure C.1: PDF curves for M-O, C-C and M-C pairs in pure liquids are unchanged by mixing.** The  
 101 coordination of  $M^{2+}$  with oxygen atoms and carbonate groups is unaffected by the composition of the liquid.  
 102 The carbon-carbon pdf curve changes when  $Mg^{2+}$  is introduced into the mix but remains a weighted average  
 103 of the two endmember components (Appendix. 4).



109 **Figure C.2: Structural packing of carbonate molecules varies systematically for Mg-bearing**  
110 **carbonate mixtures.** Shown below are pdf curves from simulations of C-C pairs (at 1100 K and 0 bar) for  
111 pure  $\text{MgCO}_3$  liquid (purple line), pure  $\text{CaCO}_3$  (yellow line) liquid and an intermediate binary composition,  
112  $\text{CaMg}(\text{CO}_3)_2$  (orange line). The black line is the C-C pdf curve of  $\text{CaMg}(\text{CO}_3)_2$  calculated from the  
113 composition-weighted average of the two end members which nearly perfectly predicts the simulated  
114 structure; this demonstrates that carbonate packing is not responsible for deviations from ideality in  $\text{CaCO}_3$ -  
115  $\text{MgCO}_3$  mixtures.



116

117